"This project has received funding from the European Union's Seventh Programme for research, technological development and demonstration under grant agreement N°603946

HEALS

Health and Environment-wide Associations based on Large population Surveys

FP7-ENV-2013- 603946

http://www.heals-eu.eu/

D5.4 Database on candidate, in vitro supported, -omics derived biomarkers, for targeted analysis

WP5 Omics, epigenetics and confirmatory in vitro analyses

Version 1

Lead beneficiary: 13 – TNO

Date: 16-10-2017

Nature: Other

Dissemination level: PU - Public

Table of Contents

Document Information

Grant Agreement Number	ENV-603946	Acronym	HEALS
Full title	Health and Environment-wide Associations based on Large population Surveys		
Project URL	http://www.heals-eu.eu/		
EU Project Officer	Tuomo Karjalainen,- Tuomo.KARJALAINEN@ec.europa.eu		

Deliverable	Number	5.4	Title	Database on candidate, in vitro supported, -omics derived biomarkers, for targeted analysis
Work Package	Number	5	Title	Omics, epigenetics and confirmatory in vitro analyses

Delivery date	Contractual	M42	Actual	16/10/2017
Status	Draft X		Final ☐	

Nature	Demonstrator ☐ Report ☐ Prototype ☐ Other X
Dissemination level	Confidential ☐ Public X

Author (Partners)	Eliandre de Oliveira, Martine Aggerbeck, Dimosthenis Sarigiannis, Rob Stierum, Bernice Schaddelee-Scholten			
Responsible Author	Rob Stierum		Email	rob.stierum@tno.nl
	Partner	TNO	Phone	+31 888661779

Document History

Name	Date	Version	Desciption

1 Introduction

The goals of the D5.4 are i) to select and define one/several candidate cohort(s) to define biomarkers of exposure in relation to the pollutants found in the biological samples; ii) to select a number of pollutants to test as a mixture in the HepaRG human hepatic in vitro model as well as in a neuronal mouse in vitro model, HT-22;; iii) to model the level of exposure in the liver, after the selection of pollutants by a PPBK approach; and iv) to provide in vitro supported OMICs data in order to correlate the biomarkers in human samples with biomarkers in the in vitro model.

Together, the outcome of this is included into a database

From WP5 meetings and previous deliverables (D5.1, 5.2 and 5.3), two existing cohorts with available biological material allowing experimental analysis were selected: REPRO PL and PHIME. REPRO PL is a Polish mother and child cohort study that evaluates the impact of exposure to several pollutants on children's health and neurodevelopment. Previous work showed an inverse association between prenatal exposure to 11 phthalate metabolites and child motor development (Polanska et al, 2014). The PHIME cohort consists of children from Italy, Greece, Slovenia and Croatia; the first studies were interested in associations between prenatal exposure to mercury/methyl mercury and either influence of polymorphisms in ABC transporter genes or CYP3A expression and neurodevelopment (Llop et al, 2014; Llop et al, 2017).

The methodology is described in more detail in chapter 2, and the results of the analyses are discussed in chapter 3. The output of this work is an Excel database of candidate, in vitro supported, - omics derived biomarkers, for targeted analysis.

2 Methodology

2.1 Measure of chemical stressors in samples from the cohorts

REPRO PL

The REPRO PL study collected information on eleven phthalate metabolites (Polanska et al. 2014) and a range of other biomarkers. Table 1 displays a selection of the studied biomarkers.

Table 1. Selection of chemical stressors studied in REPRO PL cohort

Chemical/ biomarker	Biological sample	Group	# of samples
Phthalate metabolites: DEHP, DiNP, and BBzP	urine	pregnant women (30-34 weeks of pregnancy) and children (age between 23-28 months)	150/150
Pb	blood and in cord blood	pregnant women (20 - 24 weeks of pregnancy) and during delivery	400
Hg	hair	pregnant women (30-34 weeks of pregnancy)	750

PHIME

An overview of the chemical stressors which have been measured in the PHIME study is presented in table 2 (Llop et al. 2014).

Table 2. Selection of biomarkers studied in PHIME cohort

Biological sample	Analyte
Hair	Total Hg, MeHg
Cord blood – whole blood	Total Hg, MeHg (samples above 1 mg/g of hair), Cd, Pb, As, Se, Mn, Cu, Zn, polymorphism
Cord blood – plasma	Se, Zn
Cord blood – serum	Fe, Mg, Ca
Milk	Total Hg, MeHg (samples above 1 mg/g of hair), Cd, Pb, As, Se, Mn, Cu, Zn
Cord tissue	Total Hg, MeHg (samples above 1 mg/g of hair)
Meconium	Total Hg, MeHg (samples above 1 mg/g of hair)

2.2 Study of metabolic pathways dysregulated by the pollutants

Data processing, statistical analysis, and metabolite identification

Concerning metabolomics on Repro-PL samples, samples are derived from a cohort of 400 mother and child urine and plasma samples. Partner AUTH has analysed the urine by both NMR (2015) and LC-HRMS (2016) platforms whilst partner FERA have analysed the plasma. The metabolomic analyses performed is described in greater detail in D5.3 Report on best practices for –omics analysis performed on human cohorts. An extensive validation of the method for untargeted metabolomics analysis using both NMR and LC-MS/MS has been carried out, and the resultant best practices have been applied to the analysis of 167 paired PHIME samples (mothers and children) that have been resampled. Data was uploaded onto the AUTH FTP server (ftp://155.207.30.151/).

Metabolites identified by LC-MS/MS analysis were determined using MZMine, an open-source software for mass-spectrometry data processing, with the main focus on LC-MS data (Katajamaa, et al., 2006). After data upload, mass spectral peaks were selected, aligned and annotated. The data were deconvoluted using the Wavelet (XCMS) algorithm to remove instrumental and chemical noise, thus providing only the biologically relevant information. The most crucial step regarding the understanding of the roles metabolites play in the composition of the adverse outcome pathway includes their identification because biological meaning can only be found if compounds are identified. Many databases that can be used for metabolites identification exist, but for ReproPL and PHIME cohorts, the ones that were used were the Human Metabolome DataBases (HMDB) (Wishart, et al., 2013) and Metlin (Smith, et al., 2005). The mass-to-charge ratio (m/z) value of a molecular ion of interest is searched against metabolite database(s). The metabolites having molecular weights within a specified tolerance to the query m/z value, which was defined as 10 ppm, were retrieved from the databases as putative identifications.

Finally, 380 and 1700 peaks were annotated in case of plasma ad urine samples from Repro-PL respectively. For PHIME cohort study the final outcome was 600 annotated peaks in case of plasma samples from mothers, while 800 metabolites were also annotated in case of childrens' plasma samples. Moreover, for PHIME cohort study 200 and 275 peaks were annotated in case of urine samples from mothers and children respectively.

In the case of raw data created by NMR analysis MestReNova (Mnova 11.0.3) (http://mestrelab.com/), was used for spectral analysis, while for the identification of metabolites it was deemed necessary to use in addition ChenoMx (http://www.chenomx.com/). Spectral analysis included the correction of the position of the reference peak sample, followed by alignment, the correction of signal intensity values (baseline correction) using the Smoother Whittaker algorithm (Carlos Cobas, et al., 2006; Jewison, et al., 2014), phase correction, which was performed with an automatic algorithm, and finally the binning or bucketing. The identification of the peaks was performed based on compounds that exist in the ChenoMx library and required the definition of pH and concentration of TSP in the buffer that was added to the samples, since these parameters define the position of the peaks (Amiot, et al., 2015; Beaudry, et al., 2016). Finally, peak integration of TSP and previously identified metabolites was done on MNOVA resulting in full identification of the metabolite peaks. In case of plasma ad urine samples from Repro-PL 49 and 40 peaks were annotated respectively. For PHIME cohort study the final outcome was 16 annotated peaks in case of plasma samples from mothers, while 17 metabolites were also annotated in case of plasma samples from children.

Biological interpretation

The next step in the downstream bioinformatics analysis was pathway mapping that revealed the roles that metabolites play in relation to each other and in biological aberrations. For both cohort studies, Repro PL and PHIME, pathway analysis was performed using the GeneSpring Pathway Architect, which can be used to map the results from single experiments onto curated pathways. This module finds relevant pathways associated with the experiment organism from the total number of pathways present in the tool pathways comprising the Biocyc, KEGG and WikiPathways databases based on similar entities (matched entities) between the pathway and the entity list. GeneSpring only reports the number of matched entities for a metabolomics experiment, so no p-values are computed for entities from metabolomics experiments to avoid a misrepresentation of the significance of matching pathways caused by the fact that the technology of a metabolomics experiment is limited to only the measured metabolites with an observable abundance in the experiment and pathways, on the other hand, are likely to contain many other metabolites that may not be present in the technology. This results in a pathway p-value computed with the technology to be higher than a more realistic p-value computed with a comprehensive reference set of global entities. The final outcome of the analysis was one list of 274 unique pathways for Repro PL cohort study and a list of 93 pathways for PHIME cohort.

2.3 Modeling of pollutant concentrations for in vitro experiments in HepaRG cells

Among the above mentioned chemical stressors in the REPRO PL cohort, the three most abundant phthalates were selected for in vitro experiments, together with two metals, methylmercury and total mercury. Modeling of concentrations in the liver extrapolated from the values in the human samples was performed with the INTEGRA model. The minimum, mean and maximum concentrations of phthalates and metals obtained with modeling are shown in Table 3.

Table 3. Concentrations of the pollutants in the human liver (modelled)

Concentration	DEHP	DiNP	BBzP	Hg	Pb
Max (nM)	2.560	4.778	0.192	17.947	27.053
Mean (nM)	0.230	0.478	0.018	4.686	8.213

Min (nM)	0.128	0.096	0.003	0.499	4.831

2.4 HepaRG cell culture, treatments and preparation of samples for various OMICS experiments (UPD)

For the in vitro cellular model(s), the human liver-derived HepaRG cell line was chosen for several reasons: i) after differentiation by DMSO, two cell types coexist in the culture (50% hepatocyte-like cells and biliary-type cells). Moreover bile ducts are present in the culture between hepatocytes, and thus it is one of the best cellular model for human liver. HepaRG are known to express all the xenosensors and xenobiotic metabolizing enzymes which can be implicated in the effects of the pollutants (Antherieu et al, 2010) and ii) these cells can be treated for a long time (several weeks) with low concentrations of the selected pollutants to mimic at best a low, semi-chronic exposure (Josséet al, 2008).

HepaRG cells were seeded at 30,000 cells/cm² and proliferated for 2 weeks in William's E media (Gibco, #11570606) containing 10% fetal calf serum (Eurobio), 50µM hydrocortisone hemisuccinate (Sigma, #H2270), 4µg/mL insulin (Sigma, #I9278), 500UI/mL penicillin streptomycin (Gibco, #11528876) and 2mM glutamine (Gibco, #11500626). To induce differentiation, 1.5% DMSO (Sigma, #D4540) was added to the media. Cells were fully differentiated within 15 days of treatment with DMSO.

Differentiated cells were trypsinized and seeded into 6 well plates at a density of 210,000 cells/cm². Seventy two hours later, the medium was changed and 48h later, treatments were started (Table 4). All pollutants were freshly prepared 3 times a week from stock solutions.

2.4.1 Preparation of mercury and methylmercury in solutions for in vitro experiments (JSI)

Standard solutions with different concentrations of THg and MeHg in 1% HNO3 in water for in vitro experiments were prepared on October 19th, 2016 and sent to partner UPD in France (Table 4). Water solutions for THg were prepared from NIST SRM 3133 Mercury Standard Solution (Lot. 061204) and for MeHg from CH3HgCl salt with appropriate dilutions.

Table 4: Standard solutions for in vitro experiments

THg (µg/mL)	**THg (nmol/mL) (µM)**	**MeHg (µg/mL)**	**MeHg (nmol/mL) (µM)**
0.5	2.49	0.5	2.49
1	4.98	1	4.98
3	14.9	3	14.9
10	49.8	10	49.8

30	149	30	149
500	2493	500	2493

2.4.2 Measure of remaining mercury and methylmercury in supernatants after 48H exposure of the HepaRG cells (JSI)

HepaRG cells were treated for 48h with 500µg/mL of TH or, 500µg/mL of MeHg (UPD). The supernatants were collected, frozen and sent to JSI for further analysis (received October 27th, 2017). The samples were analyzed immediately of receipt using the following apparatus: the results for T-Hg in samples were obtained by cold vapour atomic absorption spectrometry (CVAAS) using two different apparatus, Semi Automatic Mercury Analyzer Model Hg-201, Sanso Seisakusho Co., LTD and DMA-80 Direct Mercury Analyzer. The results for MeHg in samples were obtained by cold vapour atomic fluorescence spectrometry (CV AFS) using automated system Tekran 2700.

2.4.2.1 Determination of mercury (THg) in samples by acid digestion / CV AAS detection

Each sample (500 µL) was transferred directly into 50 mL volumetric flasks. After addition of 2 mL of mixture HNO3/HClO4 (1:1) and 5 mL of H2SO4 samples were digested by heating at 230-250 °C on a hot plate for 20 minutes. After cooling, the digested samples were filled up to the 50 mL mark with Milli-Q water. The same procedure (reagents without sample) was applied for blank sample. An aliquot of sample is then transferred to the reaction vessel, reduced with SnCl2 and aerated with outside air until equilibrium of mercury vapor is reached. During this circulation, acid gases leaving the sample solution are removed by acid gas trap containing 10% NaOH solution. After that, the mercury vapor is introduced to the absorption cell by turning the four-way valve and measured by cold vapor atomic absorption spectrometry (CV AAS - Semi Automatic Mercury Analyzer Model Hg-201, Sanso Seisakusho Co., LTD). Analytical measurements were checked with analysis of Standard Reference Material DOLT-4 dogfish liver. The results are presented in Table 5. The detection limit of the procedure is 0,2 ng/L. The reproducibility of the method is 5 to 10%. Estimated uncertainty with a coverage factor k=2 was 12,6%.

Table 5. Table of results of analytical measurements checked with analysis of Standard Reference Material DOLT-4 dogfish liver.

CRM	**Reference value**	**Measured value (mean value and SD of 3replicates)**
DOLT-4 (THg)	2.58 ± 0.22 (mg/kg)	2.61 ± 0.01 (mg/kg)
PT-WB1 (MeHg)	5.8 ± 0.5 (µg/kg)	5.67 ± 0.31 (µg/kg)

2.4.2.2 Determination of methylmercury (MeHg) by acid dissolution/aqueous phase ethylation /isothermal GC/CV AFS detection TEKRAN 2700

Each sample (200 µL) was weight into the 30 mL glass tubes and 10 mL of 4M HNO3 was added. The samples were than digested at 67°C over night. After cooling, the digested samples were diluted up to the 30 mL mark with Milli-Q water. An aliquot of the digested sample was then added to measuring glass vials and pH was adjusted to be 4.6 with addition of citrate buffer. 30 µL of 1% NaBEt4 was added in

the measuring vials, the vials were capped and placed into the automated system TEKRAN 2700 with an auto sampler. Ethylated MeHg as ethylmethylmercury was purged onto Tenax trap and was thermally desorbed (180°C) onto isothermal GC column. Hg species were converted to Hg0 by pyrolysis at 600°C and measured by cold vapour atomic fluorescence detector (CVAFS). Analytical measurements were checked with analysis of Control Material PT-WB1 whole blood. The results are presented in Table 5. The detection limit of the procedure is 0.02 ng/g. Expanded uncertainty with a coverage factor k=2 was 10%. As shown in Table 6, the values of the remaining total mercury (THg) or methylmercury (MeHg) after exposure of the cells did not differ significantly from the original concentration applied on the cells (500 ng/mL of either Thg or MeHg). Methylmercury, thus was not metabolized by the cells.

Table 6. Total and methyl mercury in samples (LOD: limit of detection)

Sample	**THg (ng/mL)***	**MeHg (ng/mL)***
control	0.125; 0.148	< LOD
1% HNO3	0.148; 0.148	<LOD
500ng/mL THg	402; 392	< LOD
500ng/mL THg	405; 397	<LOD
500ng/mL MeHg	579; 533; 521	511; 502
500ng/mL MeHg	654; 636	456; 456

2.4.3 Viability of cells during treatments

Before performing the actual experiments, we verified whether the mixtures used were cytotoxic for the HepaRG cells after 3 weeks treatment with both mixtures (M1 and M2, see Table 7). Two tests were used. The CellTiter 96 Aqueous One Solution Cell Proliferation Assay (Promega), based on the formation of colored formazan from MTS tetrazolium compound (Owen's reagent), was used as a cytotoxic assay. Experiments were performed in triplicate in three independent cell cultures. Apoptosis/necrosis was also measured in the same cells using the PE Annexin V Apoptosis Detection Kit (BD Biosciences). Annexin V staining (here coupled to the Phytocoerythrin (PE) fluorochrome) precedes the loss of membrane integrity which accompanies the latest stages of cell death resulting from either apoptotic or necrotic processes. The assays were performed in 3 independent cultures, using a BD FACS Canto II apparatus.

Table 7. Pollutants used in in vitro experiments

Solvent	Compound	Final concentration Mix1 (M1)	Final concentration Mix2 (M2)	MW
DMSO	DEHP	2.5nM	25nM	390.56
	Bis(2-ethylhexyl) phthalate Sigma # 36735			
	DiNP	5nM	50nM	418.61
	Diisononyl phthalate CAS Number: 28553-12-0 Sigma #376663			
	BBzP	0.2nM	2nM	312.36
	Benzyle butyle phthalate CAS Number: 85-68-7 Sigma #308501			
H2O	PbNO3	30nM	300nM	331.2
	THg	1ng/mL	10ng/mL	
	MeHg	1ng/mL	10ng/mL	

2.4.4 Treatments for OMICs experiments

All phthalates were prepared accordingly: 1µL of stock solution + 999µL DMSO for M2; 20µL of M2 + 180µL DMSO for M1. PbNO3 was diluted 1/10: 20µL of 300µM + 180µL H2O. Methylmercury (MeHg) and total mercury (Hg(II) + MeHg) solutions were provided by the IJS partner as described above.

Every other day, media was changed and pollutants, prepared extemporaneously, were added (1µL for each pollutant/mL; total of 3mL/well). After 1, 2 or 3 weeks of treatments, the cells (or medium) were recovered for the OMICs analyses. The same cells were treated in parallel plates for the various OMICs procedure.

2.4.4.1 Preparation of samples for transcriptomics

Media was discarded and 350µL of RLT plus lysis buffer (Qiagen) with 10% β-mercaptoethanol was added (just before the extraction) into each well of a 6 well plate well and frozen at -20°C until RNA extraction. RNA was extracted with RNeasy Mini kit (Qiagen) on a Qiacube automate.

2.4.4.2 Preparation of samples for proteomics

One mL of media was kept and frozen at -20°C. Cells were washed 5 times with ice cold PBS. One hundred and fifty µL of proteomic buffer ((8M urea, 0.1%SDS, 50mM ammonium bicarbonate) was subsequently added into each well of a 6 well plate. Cells were scrapped with a cell scrapper and transferred into a 1.5mL Eppendorf tube. The lysate was centrifuged at 13000g for 30min at 4°C. The supernatant was transferred to a fresh tube and kept at -20°C. Samples were sent in dry ice to the CERETOX partner for proteomic analysis.

2.4.4.3 Preparation of samples for metabolomics

One mL of media was kept and frozen in liquid nitrogen. Cells were washed 5 times with ice cold PBS. One mL of LS/MS grade methanol was added, followed by 1mL of LS/MS grade H2O. Cells were scrapped with a cell scrapper and transferred into a 15mL falcon tube. Four mL of chloroform was added followed by vortex mixing. The mixture was incubated for 30 min on ice and 2mL of LS/MS grade H2O were added. After centrifugation at 3000g for 20min at 4°C (no brake), the upper and lower phases were transferred respectively into 1.5mL Eppendorf tubes (for each condition, 2 aliquots of 1mL) and frozen in liquid nitrogen. All samples (supernatants and extracted metabolites) were kept at -80°C. Samples were sent in dry ice to AUTH for metabolomics analysis. Some samples were lost during the transport and new samples will be send in October 2017.

2.5 Downstream omics analysis

2.5.1 Transcriptomic data Analysis using Cochin platform (UPD)

The quality of the mRNA was assessed (RIN>9) and the microarray experiments were performed at the University Paris Descartes Cochin facility (Affymetrix GeneChip HuGene 2_0-st). The data from the .CEL files were normalized with the algorithm GCRMA (Partek). The used EntrezGene annotations originate from Bainarray (Version 21)1. There is a $p<0.05$ statistically different expression of the genes which are regulated with the mixture compared to the HNO3 control.

[1] http://brainarray.mbni.med.umich.edu/Brainarray/Database/CustomCDF/21.0.0/entrezg.asp

2.5.2 Transcriptomic data analysis using GeneSpring GX software (AUTH)

Raw data was analyzed using GeneSpring GX 14.9 (Agilent Technologies) with the raw data files (.cel) of the Affymetrix Human 2_0-st chip imported into the software. The RAM (Robust Multichip Averaging) algorithm was used to normalize the data where it was subjected to quantile normalization with a median of all samples taken for baseline transformation. Fold change analysis was used to identify genes with expression ratios or differences between mixture 1 and solvent control, as well between mixture 2 and solvent control, that are outside of a given cut-off or threshold. The ratio between the two conditions was calculated using the equation (Fold change = mixture 1 (or mixture 2)/solvent control). The resultant list of genes differentially expressed between the two parameters were filtered to include only those that expressed absolute fold change greater than two-fold. Clustering is a way to visualize differences between samples based on their overall gene expression profiles, represented by a heat map depicting the expression of analyzed genes in each sample. The U-Matrix view is used to display results of the SOM clustering algorithm.

The outcome of the transcriptomics analysis using GeneSpring GX is included into database.

2.5.3 Proteomics for HepaRG cells

2.5.3.1 Sample preparation

In order to perform the proteomics analyses the total protein content of the supernatants of the cellular extracts was quantified using Micro BCA™ Protein Assay Kit (Thermo Scientific). Then, thirty µg of each sample (five biological replicate of each condition) were digested with trypsin using the FASP (Filter-Aided Sample Prep) digestion approach (Wisniewski et al 2009). Briefly, samples were diluted to 270 µL with 50 mM ammonium bicarbonate (ABC)/8M urea solution and pH checked (8.0-8.5). Immediately, samples were reduced with 20 mM dithithreitol (DTT) (90 min, 32°C), and alkylated with 30mM iodoacetamide (IAA) (RT, 30 minutes in the dark). Afterwards, samples were loaded onto the Amicon Ultra (filter 10KDa, 0.5 mL, Millipore) to remove interfering compounds and substances by 4 rounds of centrifugations (12000 g, 30 min, RT) and washed (300 µL of 50 mM ABC/8M urea and 50 mM ABC, pH 8.0-8.5). The sample protein was digested with 1.2 µg of trypsin/sample during 2 h (Promega, trypsin sequencing grade 32oC, pH 8.0) and then re-digested additionally for 16 h (32oC, pH 8.0) with 0.6 µg of trypsin/sample. The resulting peptide mixture was recovered by 3 rounds of centrifugation and washes (300 µL 50 mM ABC and 10% acetonitrile), dried-down on a SpeedVac vacuum system and cleaned-up/desalted in a C18 tip (P200 Toptip, PolyLC), as per manufacturer's indications. The peptide solution was dried in a SpeedVac system and kept at -20°C until further analysis by LC-MS/MS.

2.5.3.3 Mass spectrometry analysis

Samples were analyzed in a nanoAcquity liquid chromatographer (Waters) coupled to a LTQ-Orbitrap Velos (Thermo Scientific) mass spectrometer. Peptides were resuspended in 2% ACN/1% FA solution and an aliquot (500 ng) was injected for their chromatographic separation. Peptides were trapped on a Symmetry C18TM trap column (5µm 180µm x 20mm; Waters), and were separated using a C18 reverse phase capillary column (75 µm Øi, 25 cm, nano Acquity, 1.7µm BEH column; Waters). The gradient used for the elution of the peptides was 1 to 35 % B in 155 minutes, followed by gradient from 35% to 45% in 20 min (A: 0.1% FA; B: 100% ACN, 0.1%FA), with a 250 nL/min flow rate. Eluted peptides were subjected to electrospray ionization in an emitter needle (PicoTipTM, New Objective) with an applied voltage of 2000V. Peptide masses (m/z 300-1700) were analyzed in data dependent mode where a full Scan MS in the Orbitrap with a resolution of 60,000 FWHM at 400m/z was obtained. Up to the 15 most abundant peptides (minimum intensity of 500 counts) were selected from each MS scan and then fragmented using CID (Collision induced dissociation) mode with 38% normalized collision energy, in the linear ion trap with helium as the collision gas. Generated Raw data files were collected with Thermo Xcalibur (v.2.2).

2.5.3.4 Data analysis

2.5.3.4.1 Proteomics data analysis using MaxQuant (CERETOX)

Label-Free Quantification and Database search

Raw data were processed with MaxQuant software (v XX). Andromeda search engine was used to search against SwissProt Human database (v_170519, including contaminants and decoy databases), under the following parameters: Enzyme: Trypsin; Missed Cleavage: 2; Fixed modifications: Carbamidomethyl; Variable modifications: Acetyl (Protein N-term), Oxidation (M); Peptide Mass Tolerance: 20 ppm; Fragment Mass Tolerance: 0.6 Da. MaxQuant Label-free Quantification (LFQ) was done using non-conflicting and Razor peptides and protein grouping. The software normalization algorithm was applied. Abundances are calculated as the area under the MS peak for every matched ion feature. In total 3350 proteins were quantified from a mean of 11800 identified peptides per sample.

Statistical analysis

Label-free quantitative data was submitted to ANOVA to compare significant differences among the mixture treatments and controls (5 conditions: Baseline, Control, HNO3, M1 and M2) A threshold of p-value was applied and the proteins showing p <=0.05 were considered. To every ANOVA comparison, a post-hoc Tukey Honest Significance Test was applied to do pairwise comparisons between the means of different treatments. Fold changes were calculated as the ratio of the mean of each treatment over control. Data was further curated applying p adjusted, q-value <0.05. Data quantitative analysis was performed by R v 3.1.2 (free software programming language and software environment for statistical computing and graphics; R Development Core Team, http://www.r-project.org/).

2.5.3.4.2 Proteomics data analysis using GeneSpring GX (AUTH)

The data analysis of the proteomics results was based on the same workflow followed for the analysis of transcriptomics data. Data was analyzed using the module of GeneSpring GX 14.9 called Mass Profiler Professional (Agilent Technologies). The data was normalized using the quantile algorithm, after the long transformation. Principal Component Analysis (PCA) was performed for the verification of the data consistency. Fold change analysis was used to identify proteins with expression ratios or differences between mixture 1 and solvent control, as well between mixture 2 and solvent control, that are outside of a 1.5 cut-off or threshold. Clustering is a way to visualize differences between samples based on their overall gene expression profiles, represented by a heat map depicting the expression of analyzed genes in each sample. The U-Matrix view is used to display results of the SOM clustering algorithm.

The outcome of the proteomics analysis using GeneSpring GX is included into database.

2.5.4 Metabolomics for HepaRG cells

2.5.4.1 Sample preparation

Briefly, 2 × 250-µl aliquots of each sample were transferred to a new tube and the aqueous extracts were dried using a Techne Sample concentrator (Time: 180 min, Temperature: 45 °C). Then, the samples were resuspended using 120 µl of solvent water/methanol in ratio of 70:30 and the extracts were transferred into new eppendorfs. The solvent also contained internal standards according to the analysis mode which were paracetamol (m/z 152.0707, 1ppm), caffeine (m/z 195.0877, 1ppm), risperidone (m/z 411.2191, 1ppm), reserpine (m/z 609.2807, 1ppm), and roxithromycin (m/z 837.5318, 1ppm) in case of ESI(+) mode, and caffeic (m/z 179.0349, 1ppm), tetrabromobisphenol A (m/z 542.7445, 1ppm), and finally reserpine (m/z 607.2661, 1ppm) in case of ESI(-) mode. For the preparation of the QC sample(s) equal volumes from each of the samples in the batch were mixed, as they were being aliquoted after extraction and resuspension.

2.5.4.2 Mass spectrometry analysis

ThermoFisher Scientific (Bremen, Germany) model LTQ Orbitrap Discovery MS with a resolution 30,000 system was used. Sample analysis is going to be carried out in positive and negative ion modes. The mass scanning range was set between 50–1000 m/z and the capillary temperature at 32°C. The flow rate for nitrogen sheath gas and auxiliary gas was 40 L/min and 8 L/min respectively. Spray voltage was 4.5 kV, with the LC–MS run in a gradient mode with two solvents. Mobile Phase A: 100% high-grade water with 0.1% formic acid and mobile phase B: 100% methanol with 0.1% formic acid: the flow rate was 400 µl/min in both positive and negative mode.

Chromatographic separations were achieved using an Acquality UPLC HSS T3 column (100 x 2.1 mm, 1.8 µm, Waters, Milford, MA, USA) maintained at a constant temperature of 40°C. The following gradient was used for both positive and negative mode: 0.1% B at 0 min, 0.1% B at 2 min, 25% B at 6 min, 80% B at 10 min, 90% B at 12 min, 99.9% B at 21 min, 99.9% B at 23 min, 0.1% B at 24 min and 0.1% B at 26 min. Two blank samples were injected before the starting QC of each run for checking the column, and ten QC pooled samples were injecting for the baseline stabilization of the LC–MS system. All samples in positive mode were run as one batch. The pooled QC sample repeated every five samples and every ten samples, a solvent blank is repeated.

Generated Raw data files were collected with Thermo Xcalibur (v.2.2).

2.5.4.3 Data analysis

Metabolites identified by LC-MS/MS analysis were determined using MZMine v2.31. After data upload, mass spectral peaks were selected, aligned and annotated. The data were deconvoluted using the Wavelet (XCMS) algorithm to remove the noise, thus providing only the biologically relevant information. Human Metabolome DataBases (HMDB) and Metlin, were used for the identification step under mass tolerance 5ppm. To obtain consistent variables, the resulting matrix was further reduced by removing peaks with more than 80% missing values (those with ion intensity = 0) among the pooled control samples. Instrument variability was determined by calculating the median RSD for the I.S of the 4 treatment conditions, while overall process variability was determined by calculating the median RSD for all the endogenous metabolites of the 4 treatment conditions. To test instrument' s performance and overall process variability, the RSD of RT, peak area and mass accuracy of each internal standard will be calculated for all the problem samples. A threshold of 30% ensured the repeatability in metabolomics data sets. The final list of annotated metabolites included 80/1134 and 76/1669 metabolites in case of negative and positive ionization mode respectively. The analytical performance was evaluated with respect to the whole metabolic pattern by using PCA. According to the PCA score plots none of the problem samples behave as outlier. In metabolomics research, it is important to reduce systematic error in experimental conditions. To ensure that metabolomics data from different studies are comparable, it is necessary to remove unwanted systematic factors by data normalization. In this study, the quantile normalization was applied using the pre-process core package, and more specific the normalize.quantiles function. The density plot for the normalized data of the distribution can be used in order to check the performance of the algorithm. The resultant list of annotated metabolites was imported into GeneSpring GX v.14.9 (Agilent Technologies), were a fold change analysis was used to identify genes with expression ratios or differences between mixture 1 and solvent control, as well between mixture 2 and solvent control, that are outside of a given cut-off or threshold. In order to organize in an efficient way genes/entities and conditions in the dataset, clustering analysis was performed on the set of entities filtered for statistically significant changes. Clustering is a way to visualize differences between samples based on their overall gene expression profiles, represented by a heat map depicting the expression of analyzed genes in each sample. The U-Matrix view is used to display results of the SOM clustering algorithm.

2.6 HT 22 cell culture, metals treatments and preparation of samples for Proteomics experiments (PCB)

In addition to the studies performed on Hepa RG cells, the mouse hippocampal neuronal cell line HT22 were included as a model to investigate the neurotoxic effects induced by metals exposure. Among various research tools, neuronal cell lines are the most commonly used in vitro model for relevant mechanistic studies. The HT-22 cells have been used as a hippocampal neuronal cell model in the study to better understand the molecular mechanisms involved in Pb-, As and MeHg - induced neurotoxicity in hippocampus. In this work, we aimed to develop a novel in vitro approach which detects neurotoxicity comprehensively, and provides mechanistic insights. For this purpose we

explored the hippocampal based HT-22 cell line with a label free mass spectrometry (LC-MS/ MS) based on a quantitative proteomic approach.

2.6.1 Culture and treatment

The HT-22 cells were a generous gift from Dr. David Schubert (The Salk Institute, La Jolla, CA). HT-22 cells were maintained in Dulbecco's modified Eagle's medium (DMEM [D6429]) containing 10% fetal bovine serum (FBS Gibco [10500-064]) and 100 U/mL penicillin, and 100 µg/mL streptomycin (Pan-Biotech- Germany) in a humidified incubator with 5% CO2 in air at 37°C (Niska et al., 2015). For all the experiments in 8 day duration cells were grown at 70- 80% confluence.

The cells were cultured in 75 cm2 cell culture flasks. For experimental purpose, cells were plated at 0.57 x 106 cells/ mL and grown for 24 hours before metal treatment. Duplicates wells of cells were treated with 10 exposure levels of Pb, Cd, As and, MeHg ranging from 10 to 100 µM, 0.5 to 7 µM, 0.6 to 12 µM, 0.4 to 4.2 µM, respectively; due to the 8 day exposure medium containing the given concentration was refreshed at 2 days interval for maintaining metal exposure. Metal stock solutions 100X were prepared in deionized distilled water (for poorly soluble PbCl2 <0.5% DMSO added) and sterilized by filtration through 0.2 µm and different concentrations of a working solution of each individual metal was prepared by prior dilution of the stock solution in phosphate buffer saline (pH = 7.4) and then applying 10% working solution on DMEM culture medium.

For the proteomics purposes, HT-22 cell cultures were treated for 8 days with sub lethal (IC10) concentrations of metals (63.5, 0.42 and 0.09 µM respectively for Pb, As and MeHg).

After exposure to the metals(or control condition culture), protein was extracted from HT-22 cells with 8 M urea, 0.1% SDS, 50 mM ammonium bicarbonate buffer. Briefly, cells were washed 5 times with ice cold PBS. One hundred and fifty µL of urea buffer were added and cells were scrapped with a cell scrapper and transferred into a 1.5mL Eppendorf tube. The lysate was centrifuged at 13000g for 30min at 4°C. The supernatant was transferred to a fresh tube and kept at -80°C.

2.6.2 Proteomics for HT 22

The sample preparation and Mass spectrometry analysis protocols were similar to the description in section 2.6.2.

2.6.2.1 Proteomics data analysis using Progenesis QI (CERETOX)

Label-Free Quantification and Database search

Raw data was processed with Progenesis QI for Proteomics software (Non-Linear Dynamics, Waters, U.S.). Pool samples mass spectra were used as alignment reference. Alignment was manually reviewed. Peak Picking was automatically done. From all the ions identified a total of 428,801 MS spectra (z > 1 and Rank < 10) were considered for database search. Mascot (v_2.3.01, Matrix Science) was used to search against SwissProt Mouse database (v_170519, including contaminants) including decoy database, under the following parameters: Enzyme: Trypsin; Missed Cleavage: 2; Fixed modifications: Carbamidomethyl (C); Variable modifications: Acetyl (Protein N-term), Oxidation (M); Peptide Mass Tolerance: 10 ppm; Fragment Mass Tolerance: 0.6 Da; Instrument type: ESI-FTICR. Progenesis Label-free Quantification (LFQ) was done using non-conflicting peptides and protein grouping, and the software normalization algorithm was applied to all proteins. Abundances are calculated as the area under the MS peak for every matched ion feature. Search results were filtered based on Peptide Ion Score≥ 40 and contaminants were removed and abundances were normalized to all proteins. In total, 3,143 proteins were quantified from 27,088 peptide ions.

Data analysis

Label-free quantitative data was submitted to ANOVA to compare significant differences among the single metal treatments and control (4 levels: Control, Methyl Mercury, Lead and Arsenic) as well as the Mixed metal treatments and control (5 levels: Control, M1, M2, M3, M4). In an alternative approach, ANOVA was also applied to compare single metal treatments and mixed metal treatments (9 levels: MeHg,

Pb, As, M1, M2, M3, M4). A threshold of p-value was applied and the proteins showing p<=0.05 OR 0.01 were considered. To every ANOVA comparison, a post-hoc Tukey Honest Significance Test was applied to do pairwise comparisons between the means of every treatment. Fold changes were calculated as the ratio of the mean of each treatment over control. Data was further curated applying the following filters: minimum 2 unique peptides used for quantitation and minimum 2-fold change. Data quantitative analysis was performed by R v 3.1.2 (free software programming language and software environment for statistical computing and graphics; R Development Core Team, http://www.r-project.org/).

3 Results

3.1 Metabolomic results from the REPRO_PL and PHIME cohorts

First of all, the imbalance between the cellular reactive oxygen species (ROS), which may be an effect of exposure to phthalates and metals, and the unability of the cell to detoxify them, leads to oxidative stress. According to literature, abnormalities in the citric acid cycle, urea cycle, and amino acid metabolism play a key role in the pathogenesis of oxidative stress (Meguid, et al., 2017; Yoshimi, et al., 2016). Glutathione, methionine, cysteine, pyruvate, N-acetylglutamic acid, β-alanine, serine, and arginine, which have been detected in samples from ReproPL and PHIME cohort studies, could play the role of candidate biomarkers for the pathogenesis of neurodevelopment due to oxidative stress. In addition, the perturbations of the identified pathways, for the homeostatic operation of which the presence of the above biomarkers is crucial must be examined as a putative underlying mechanism. Some of these identified pathways are: S-methyl-5-thio-Alpha-D-ribose 1-phosphate degradation, folate metabolism, serotonin degradation, taurine biosynthesis, citrulline-nitric oxide cycle etc.

Glycolysis, Tricarboxylic Acid Cycle (TCA), and mitochondrial electron transport are the main pathways that constitute mitochondrial respiration; thus, the down-regulated activity of these metabolic pathways collectively suggested an impaired mitochondrial function at an early pregnancy stage, after the exposure to phthalates and metals. Mitochondria are central to energy metabolism and cellular signaling and are important to the synthesis of nucleotides, active transport processes, cell motility, and cell proliferation. The dysfunction of mitochondria along with the disturbed glycolysis may be implicated in neurodevelopment disorders according to clinical data and molecular investigations (Zheng, et al., 2011). Glycolysis/Gluconeogenesis and TCA cycle were ones of the identified perturbed pathways in both ReproPL and PHIME samples. Metabolomics analysis of ReproPL plasma samples revealed the presence of D-fructose 1,6-bisphosphate, b-Glucose, and acetate, which are intermediates products of glycolysis, while the analysis of urine samples of PHIME revealed the presence of oxoglutaric acid and oxalosuccinic acid, which play a key role in both TCA cycle and glycolysis.

Exposure to endocrine disrupting chemicals (EDCs) is associated with the citric acid cycle and more specific with oxidation by which fatty acids are metabolized to acetyl-CoA, which enters the citric acid cycle, indicating the possibility of disruption of mitochondrial respiration. Oxidation of fatty acids could theoretically influence electron flow by the former pathway, leading to altered ROS levels (Donohoe, et al., 2012; Jones, et al., 2000). NMR analysis of plasma samples from ReproPL and PHIME, as well as the analysis of urine samples with LC-MS/MS pointed out the presence of succinate, 2-oxoglutarate, formate, isocitrate, oxoglutaric acid, glycerol and L-carnitine. In addition, pathway analysis revealed that the previous metabolites were the matched entities for the metabolic pathways of fatty acid alpha-oxidation.

Moreover, dysfunction in carnitine metabolism may affect calcium homeostasis, which will be involved in mitochondrial oxidative phosphorylation that leads to neurodevelopmental disorders (Zheng, et al., 2011). Pathway analysis showed that the metabolic pathway of L-carnitine biosynthesis was statistical significant perturbed, may be due to the occurrence of 2-oxoglutarate, succinate in Repro plasma samples and the presence of L-carnitine in both ReproPL and PHIME children samples.

EDCs can also disrupt the synthesis, transport, and release of many neurotransmitters, including dopamine, serotonin, norepinephrine, and glutamate, which play key roles in modulating behavior, cognition, learning, and memory (Schug, et al., 2015). According to both the literature search and the pathway analysis on our own samples, perturbations on the main pathways of dopamine, serotonin, norepinephrine, and glutamate metabolism could lead to identifying potential biomarkers of neurodevelopment. Metabolites that could be considered as candidate biomarkers, according to metabolomics analysis of samples, are: homovanillic acid, L-tyrosine, L-tryptophan, 5-hydroxy-L-tryptophan, cysteine, 5-hydroxy-L-tryptophan, oxoglutaric acid, L-aspartic acid, glutamate, fumarate, succinate, 5-hydroxyindole acetate, dopamine, and melatonine.

Peroxisome proliferator activated receptors (PPARs) are ligand activated transcription factors with crucial functions in lipid homeostasis, glucose metabolism, anti-inflammatory processes, placental development, and are involved in cognitive functions and neurodegenerative diseases (Zhen, et al., 2007). The following biomarker, that have been detected in urine samples from ReproPL study, arise from PPARalpha

effects on tryptophan, corticosterone, fatty acid metabolism and on glucuronidation: Hippurate, 2,8-dihydroxyquinoline-beta-d-glucuronide, 11beta-hydroxy-3,20-dioxopregn-4-en-21-oic acid, 11beta,20-dihydroxy-3-oxopregn-4-en-21-oic acid, nicotinamide, nicotinamide 1-oxide, 1-methylnicotinamide, xanthurenic acid, hexanoylglycine, phenylpropionylglycine, and cinnamoylglycine.

3.2 Viability of the HepaRG cells treated with the mixture of pollutants

Since the concentrations obtained after modeling were low compared to concentrations used in most in vitro experiments (usually in the µM to mM range for phthalates), it was decided to treat the cells with the maximum concentrations modeled as well as with 10-times higher concentrations (see Table 4 compared to Table 3). In preliminary experiments, it was first tested if these mixtures impacted the viability of the cells, using two techniques. With the MTS assay, none of the mixtures affected cell viability, compared to both the control and the HNO3 solvent samples (Figure 1). In the apoptosis/necrosis assay, further apoptosis/necrosis was not seen in the treated M1 and M2 samples compared to the control and the HNO3 solvent samples, as shown in Figure 2 (about 10% cell death). Altogether, the results show that none of the mixtures was toxic for the HepaRG cells in the conditions used.

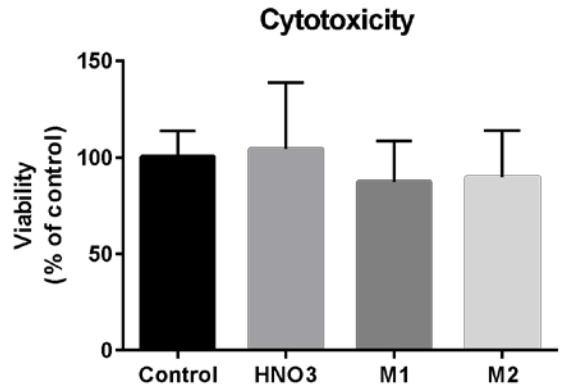

Figure 1. Cytotoxicity after 3 weeks of treatment with both mixtures of the HepaRG cells. The HepaRG cells were treated for 3 weeks with either the M1 or M2 mixtures as well as treatment with the solvent (HNO3) and compared to the control. The MTS assays were performed in triplicate and the cell viability in the control was arbitrarily set at 100%.

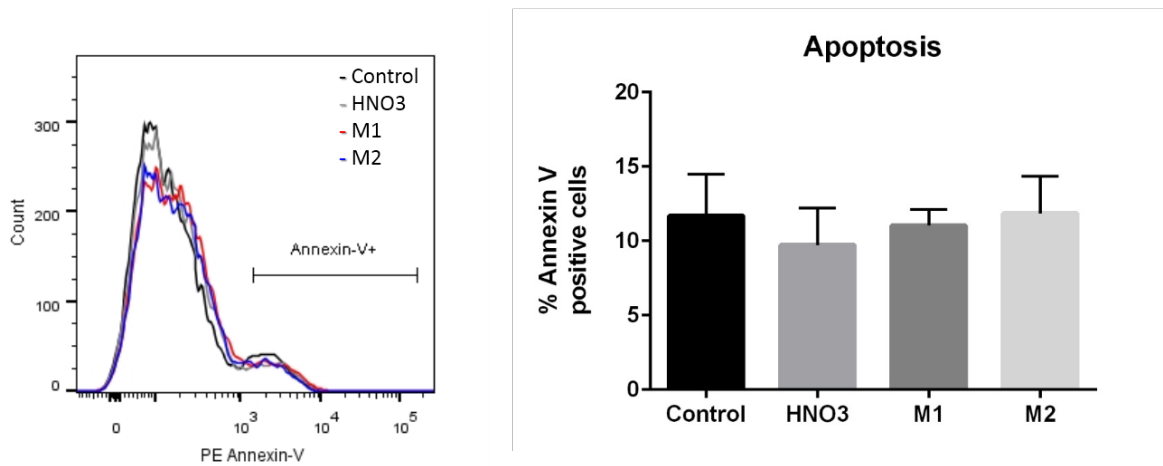

Figure 2. Apoptosis/necrosis after 3 weeks of treatment with both mixtures of the HepaRG cells. The HepaRG cells were treated for 3 weeks with either the M1 or M2 mixtures as well as treatment with the solvent (HNO3) and compared to the control. The

apoptosis/necrosis assays were performed in triplicate in a BD FACS Canto II apparatus. Left panel, the number of cells are shown in ordinate whereas the annexin-V+ bar represents the dying cells (abscissa). Right panel represents the quantification of the cells in the various conditions.

3.3 OMICS results of in vitro experiments in HepaRG cells.

3.3.1 Transcriptomics of in vitro experiments in HepaRG cells

3.3.1.1 Transcriptomic analysis using XX software

Since the mixtures M1 and M2 tested did not modify the cell viability, 3 week-treatments were performed. mRNA was prepared and the global gene expression was analyzed with the Affymetrix microarray technique. A first analysis was performed with all the 5 samples tested (passages 13 to 15), using a fold change greater than 1.5. The names of the genes and the expression of up- or down-regulation, is indicated in Tables 8 and 9, respectively. The known roles of these genes can be found in the annex table (the Excel database). As shown in Table 10, the expression of those genes was either increased (, left) or decreased (right) by each concentration of the mixture. Some genes displayed a regulation with the 2 concentrations tested, which strengthens the results obtained (genes in red).

Table 8. Acronymes and names of up-regulated genes

Gene acronyme	Gene name
PCK1	phosphoenol pyruvate carboxykinase 1
SCGN	segretagogin
CYP2A6	cytochrome P450 2A6
UGT1A7	UDP-glycosyltransferase 1A7
SNRPN	Small Nuclear Ribonucleoprotein Polypeptide N
UGT1A4	UDP-glycosyltransferase 1A4
RDH14	Retinol Dehydrogenase 14
CYP2B6	cytochrome P450 2B6

BBOX1	gamma butyrobetaine hydroxylase
FAM222A	family with sequence similarity 222 member A
SULT2A1	Sulfotransferase2A1
CYP17A1	cytochrome P45017A1
FAM133B	family with sequence similarity 133 member B
CA11	carbonic anhydrase 11
HMOX1	heme oxygenase1

Table 9. Acronymes and names of down-regulated genes

Gene acronyme	Gene name
AHSG	alpha-2-HS-glycoprotein or fetuin A
CA9	carbonic anhydrase 9
CRP	c-reactive protein
DPT	dermatopontin
SPP2	Secreted Phosphoprotein 2
DCN	decorin
H19	long non coding RNA H19

OMD	osteomodulin
TMEM45A	Transmembrane Protein 45A
IGFBP1	Insulin-like growth factor-binding protein 1
CPS1	Carbamoyl phosphate synthetase 1
CCL20	Chemokine (C-C motif) ligand 20
CASP14	caspase 14
CXCL13	chemokine (C-X-C motif) ligand 13

Table 10. Up and down-regulated genes by the two mixtures tested in HepaRG cells found within all the 5 tested biological samples (passages 13 to 15). Genes in red represent genes differentially regulated with the two mixtures (fold change greater than 1.5)

up-regulated genes (name)	up-regulated genes (fold) by M1 mixture	up-regulated genes (fold) by M2 mixture		down-regulated genes (name)	down-regulated genes (fold) by M1 mixture	down-regulated genes (fold) by M2 mixture
PCK1	1.8	-		AHSG	-3.02	-3.164
SCGN	1.76	1.712		CA9	-2.86	-
CYP2A6	1.75	-		CRP	-2.51	-2.438
UGT1A7	1.7	-		DPT	-2.34	-2.786
SNRPN	1.65	1.525		SPP2	-2.12	-1.957
UGT1A4	1.59	1.537		DCN	-2.08	-
RDH14	1.59	-		H19	-2.07	-1.993
CYP2B6	1.59	1.486		OMD	-2.05	-2.524
BBOX1	1.52	1.77		TMEM45A	-1.99	-
FAM222A	1.52	-		IGFBP1	-1.94	-
SULT2A1	-	1.587		CPS1	-	-2.504
CYP17A1	-	1.542		CCL20	-	-2.212
FAM133B	-	1.507		CASP14	-	-2.107
CA11	-	1.502		CXCL13	-	-2.018
HMOX1	-	1.485				

Among the up-regulated genes, BBOX1 is involved in carnitine metabolism, a key molecule in energy metabolism which activates fatty acid transport in the mitochondria (Rigault et al, 2013) and dysfunction in its metabolism has been linked with neurodevelopmental disorders. Indeed, recently, an homozygous deletion of the BBOX1 and fibin genes has been linked to microcephaly, speech delay, growth retardation and minor facial anomalies (Rashidi-Nezhad et al, 2014). Another up-regulated gene was SCGN which encodes secretagogin, a

multifunctional Ca binding protein (Kandelwal et al, 2016), is implicated in diabetes (Yang et al, 2016) and expressed in GABAergic neurons (Raju et al, 2017) and a recent report describes the association of its lower plasma level in autistic children, compared to healthy controls (Alhowikan et al, 2017).

AHSG, the mRNA expression of which is down-regulated in the in vitro study, has been shown to be down-regulated in patients with Alzheimer's disease (Kitamura et al, 2017) whereas its high level in serum has been associated with diabetes (Aroner et al, 2016). Moreover, an homozygous missense mutation has been associated with the alopecia and mental retardation rare syndrome (Reza Sailani et al, 2017)

Two genes implicated in imprinting in the mouse are up-regulated (SNRPN) (Chebotarev et al, 2014), or down-regulated (H19) (Larocca et al, 2014) in the HepaRG cells. Among the genes, which are up-regulated with both concentrations of pollutants in HepaRG cells, CYP2B6, a gene which was shown to be up-regulated in human hepatocytes by DEHP, through the constitutive androstane receptor (CAR) (Eveillard et al, 2009) as well as UGT1A4 are xenobiotic metabolizing enzymes. Finally, DPT and SPP2 also are both down-regulated by the 2 treatments.

If one looks at the top canonical pathways or regulators unraveled by the ingenuity software, LPS/IL1 mediated inhibition of RXR function is found for both conditions of treatment, with a role in inflammation with leptin and AhR found as top upstream regulators (see annex for more details on pathways).

3.3.2 Proteomics results of in vitro experiments in HepaRG cells

From more than 3000 proteins detected by mass spectrometry, 33 changed abundance significantly when we compared the cells treated with the mixtures M1 or M2 with the cells exposed to the solvent HNO3 (Table 14). Most of these proteins were significantly deregulated in the treatment with M2, but not with M1, although tendencies of changes were similar in both treatments. In order to make easier to readers, positive and negative fold changes are respectively marked in red and blue in table 11.

We used the String tools (http://string-db.org/) in order to perform a pathway analysis on these deregulated proteins. The figure 3 shows the network formed by those proteins. The blue circles represented the proteins related to Carbon metabolism (FDR = 1.04e-09) and the red ones represent the proteins related to Fatty Acid degradation (FDR =7.04e-09), according to KEGG database.

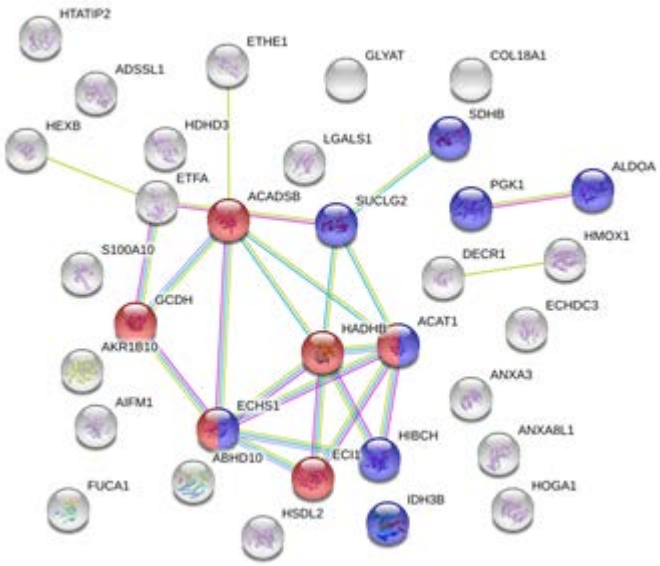

Figure 1: Network formed by the 33 deregulated proteins (String, http://string-db.org/)

Table 11: Proteins changing significantly the abundance under M1 or M2 treatments

Accession	Protein names	Gene names	FC M1/HNO3	p-adj M1-HNO3	FC M2/HNO3	p-adj M2-HNO3
P09601	Heme oxygenase 1	HMOX1	1,64	0,114	2,01	0,010
Q92947	Glutaryl-CoA dehydrogenase, mitochondrial	GCDH	1,46	0,192	1,71	0,027
O43837	Isocitrate dehydrogenase [NAD] subunit beta, mitochondrial	IDH3B	1,43	0,037	1,61	0,007
Q96DC8	Enoyl-CoA hydratase domain-containing protein 3, mitochondrial	ECHDC3	1,43	0,070	1,58	0,012
Q6IB77	Glycine N-acyltransferase	GLYAT	1,51	0,057	1,54	0,045
Q9BUP3	Oxidoreductase HTATIP2	HTATIP2	1,21	0,548	1,50	0,037
Q96I99	Succinyl-CoA ligase [GDP-forming] subunit beta, mitochondrial	SUCLG2	1,34	0,125	1,49	0,016
P04066	Tissue alpha-L-fucosidase	FUCA1	1,39	0,044	1,44	0,023
P30084	Enoyl-CoA hydratase, mitochondrial	ECHS1	1,14	0,781	1,43	0,023
Q9BSH5	Haloacid dehalogenase-like hydrolase domain-containing protein 3	HDHD3	1,21	0,334	1,42	0,010
Q9NUJ1	Mycophenolic acid acyl-glucuronide esterase, mitochondrial	ABHD10	1,29	0,154	1,41	0,027

Accession	Protein names	Gene names	FC M1/HNO3	p-adj M1-HNO3	FC M2/HNO3	p-adj M2-HNO3
Q86XE5	4-hydroxy-2-oxoglutarate aldolase, mitochondrial	HOGA1	1,17	0,497	1,41	0,031
P42126	Enoyl-CoA delta isomerase 1, mitochondrial	ECI1	1,40	0,053	1,40	0,043
P07686	Beta-hexosaminidase subunit beta	HEXB	1,25	0,269	1,39	0,038
Q6NVY1	3-hydroxyisobutyryl-CoA hydrolase, mitochondrial	HIBCH	1,23	0,272	1,39	0,021
P24752	Acetyl-CoA acetyltransferase, mitochondrial	ACAT1	1,25	0,263	1,38	0,037
P55084	Trifunctional enzyme subunit beta, mitochondrial;3-ketoacyl-CoA thiolase	HADHB	1,41	0,015	1,37	0,022
O95831	Apoptosis-inducing factor 1, mitochondrial	AIFM1	1,20	0,371	1,37	0,044
P13804	Electron transfer flavoprotein subunit alpha, mitochondrial	ETFA	1,32	0,074	1,35	0,037
P45954	Short/branched chain specific acyl-CoA dehydrogenase, mitochondrial	ACADSB	1,26	0,056	1,35	0,008
P21912	Succinate dehydrogenase [ubiquinone] iron-sulfur subunit, mitochondrial	SDHB	1,25	0,125	1,34	0,037
Q6YN16	Hydroxysteroid dehydrogenase-like protein 2	HSDL2	1,18	0,254	1,32	0,024

Accession	Protein names	Gene names	FC M1/HNO3	p-adj M1-HNO3	FC M2/HNO3	p-adj M2-HNO3
Q16698	2,4-dienoyl-CoA reductase, mitochondrial	DECR1	1,17	0,311	1,31	0,030
O95571	Persulfide dioxygenase ETHE1, mitochondrial	ETHE1	1,49	0,012	1,31	0,133
O60218	Aldo-keto reductase family 1 member B10	AKR1B10	1,12	0,442	1,28	0,009
P60903	Protein S100-A10	S100A10	-1,43	0,033	-1,37	0,095
P39060	Collagen alpha-1(XVIII) chain;Endostatin	COL18A1	-1,22	0,286	-1,38	0,028
P04075	Fructose-bisphosphate aldolase A	ALDOA	-1,26	0,211	-1,44	0,023
P00558	Phosphoglycerate kinase 1	PGK1	-1,25	0,249	-1,47	0,012
P12429	Annexin A3	ANXA3	-1,29	0,271	-1,56	0,026
Q8N142	Adenylosuccinate synthetase isozyme 1	ADSSL1	-1,24	0,192	-1,58	0,001
Q5VT79	Annexin A8-like protein 2	ANXA8L2	-1,60	0,037	-1,91	0,004
P09382	Galectin-1	LGALS1	-1,94	0,040	-2,10	0,024

Red: up-regulated in the mixtures; Blue down-regulated in the mixtures

3.3.3 Metabolomics results of in vitro experiments in HepaRG cells

From more than 1410 metabolites detected by LC-MS/MS, characterized by statistical significantly regulation when compared the cells treated with the mixtures M1 or M2 with the cells exposed to the solvent HNO3, 74 metabolites were annotated (Table 12). In addition, 37 and 35 metabolites were down-regulated in case of M1 and M2 respectively, while 37 and 39 metabolites were up-regulated in case of M1

and M2 respectively. Moreover, 14 metabolites were significantly down-regulated in the treatment with M1, but up-regulated in the treatment with M2, and 12 metabolites were significantly up-regulated in the treatment with M1, but down-regulated in the treatment with M2.

Table 12. Regulation of annotated metabolites by the two mixtures tested in HepaRG cells.

Compound	Log FC ([M1] vs [HNO3]) : Normalized	Regulation ([M1] vs [HNO3]) : Normalized	Log FC ([M2] vs [HNO3]) : Normalized	Regulation ([M2] vs [HNO3]) : Normalized
(R)-2-Benzylsuccinate	-2.38	down	-2.52	down
(R)-2-methoxyhexadecanoic acid	-3.32	down	0.66	up
(R)-3-Hydroxy-5-phenylpentanoic acid	-1.49	down	-0.48	down
12,13-DiHOME(9)	1.08	up	-2.53	down
12-Hydroxydodecanoic acid	3.98	up	2.48	up
14-hydroxy palmitic acid	3.98	up	2.48	up
1-tetradecanoyl-sn-glycero-3-phosphate	-1.49	down	-0.48	down
2-Dodecylbenzenesulfonic acid	0.34	up	-1.72	down
2-hydroxystearate	-1.10	down	-1.33	down
2-Methylacetophenone	-1.49	down	-0.48	down
3-Hydroxyglabrol	-3.32	down	0.66	up
3-Methylsubericacid	-0.52	down	2.52	up
4-Hydroxyphenylacetaldehyde	3.98	up	2.48	up
4-Methoxybenzaldehyde	4.88	up	4.66	up
7-Methoxypraecansone B	1.08	up	-2.53	down
9-keto stearic acid	1.08	up	-2.53	down
Aesculetin	-0.52	down	2.52	up
Avenic acid A	3.98	up	2.48	up
Avocadene	-0.52	down	2.52	up
Avocadene 4-acetate	-1.10	down	-1.33	down
Azelaic acid	2.02	up	2.26	up
Bis(1-methylethyl) hexanedioate	-3.32	down	0.65	up
Carinol	1.08	up	-2.53	down
Cholestane-3,7,12,25-tetrol-3-glucuronide	-0.33	down	-1.36	down
Cubebinone	3.98	up	2.48	up
D-Glutamine	1.55	up	1.69	up
diisobutyl phthalate	-2.38	down	-2.52	down
Dodecanedioic acid	-0.52	down	2.53	up
Eremopetasinorol	3.98	up	2.48	up
Eupahyssopin	2.28	up	0.99	up
Farnesiferol A	3.98	up	2.48	up
Foeniculoside IX	-0.52	down	2.52	up
gibberellin A19	1.63	up	-2.05	down

Compound	Log FC ([M1] vs [HNO3]) : Normalized	Regulation ([M1] vs [HNO3]) : Normalized	Log FC ([M2] vs [HNO3]) : Normalized	Regulation ([M2] vs [HNO3]) : Normalized
gibberellin A29	-1.80	down	-0.36	down
Gibberellin Ga115	-1.488	down	-0.48	down
Glutathione	2.87	up	1.75	up
Glycerylphosphorylethanolamine	0.52	up	1.13	up
Glycodiazine	1.26	up	0.95	up
Glyflavanone A	2.44	up	2.50	up
Juniperic acid	3.03	up	0.65	up
Kukoamine A	-0.15	down	-1.74	down
Lactapiperanol D	-3.32	down	0.65	up
lambda isostearic acid	3.98	up	2.48	up
L-Glutamic acid	-0.52	down	2.52	up
L-Glutamine	-3.32	down	0.65	up
Lisuride	2.04	up	-2.06	down
L-Olivosyl-oleandolide	-3.32	down	0.66	up
LPA(0:0/16:0)	-1.38	down	-0.35	down
LPA(18:0/0:0)	-1.10	down	-1.33	down
Lyratol	-3.73	down	-0.24	down
Methyl dihydrojasmonate	1.08	up	-2.53	down
Mitotane	-1.82	down	1.10	up
Monobutylphthalate	3.03	up	0.65	up
Monoethylhexyl phthalic acid	-1.49	down	-0.48	down
Myricatomentoside II	-1.10	down	-1.33	down
Myricetin 3-(2'',3'',4''-triacetylxyloside)	-1.17	down	-1.01	down
N-Undecylbenzenesulfonic acid	-1.29	down	-1.14	down
omega-hydroxy hendecanoic acid	1.08	up	-2.53	down
PA(13:0/13:0)	2.71	up	2.53	up
PC(15:0/20:5(5Z,8Z,11Z,14Z,17Z))	1.08	up	-2.53	down
Pentadecanedioic acid	-2.38	down	-2.52	down
phorbol 13-acetate	-1.16	down	3.35	up
Phosphocreatine	1.28	up	0.38	up
Propylene glycol stearate	-2.38	down	-2.52	down
Pyrrolidonecarboxylic acid	1.26	up	3.83	up
Ricinelaidic acid	3.60	up	1.83	up
Selenocystathionine	3.03	up	0.65	up
Sodium Tetradecyl Sulfate	2.43	up	-2.05	down
Taurochenodesoxycholic acid	1.08	up	-2.53	down
Tetracosanoic acid	-1.49	down	-0.48	down

Compound	Log FC ([M1] vs [HNO3]) : Normalized	Regulation ([M1] vs [HNO3]) : Normalized	Log FC ([M2] vs [HNO3]) : Normalized	Regulation ([M2] vs [HNO3]) : Normalized
Uridine diphosphategalactose	0.030115366	up	1.09	up
Uridine diphosphate-N-acetylgalactosamine	1.8081741	up	2.15	up
Vaccenic acid	-2.378685	down	-2.52	down
Valtratum	-0.6383985	down	-2.49	down

3.3.4 Multi-omics Pathway Analysis

Differentially expressed genes, proteins and metabolites were co-mapped on available pathways from WikiPathways, BioCyC, and KEGG databases, using the module Pathway Architect of GeneSpring. No p-values were computed for entities from metabolomics and proteomics experiments during a multi-omics experiment to avoid a misrepresentation of the significance of matching pathways caused by the fact that GeneSpring uses the technology (All Entities list) as a reference for p-value computation. The technology of a metabolomics or a proteomics experiment is limited to only the measured metabolites with an observable abundance in the experiment. Pathways on the other hand are likely to contain many other metabolites that may not be present in the technology. This results in a pathway p-value computed with the technology as reference to be higher than a more realistic p-value computed with a comprehensive reference set of global entities. To avoid this apparent increase in significance, GeneSpring only reports the number of matched entities for a metabolomics or proteomics experiment.

According to multi-omics pathway analysis glutathione-mediated detoxification I has been identified across all the three multiple layers. Moreover, the metabolic pathways of folate metabolism and urea has been identified across transcriptomics and proteomics experiments. Imbalance between the cellular ROS and the ability of the cell to detoxify them, lead to oxidative stress. In case that the brain is highly exposed to increased oxidative stress due to the presence of excitatory amino acids whose metabolism ends with the production of ROS causing neuronal damage. According to literature, abnormalities in the citric acid cycle, urea cycle, and amino acid metabolism play a key role in the pathogenesis of oxidative stress, which may be an effect of exposure to phthalates and metals. Co-exposure to phthalates and heavy metals may result in the imbalance between the cellular ROS and the ability of the cell to detoxify them (Meguid, et al., 2017; Yoshimi, et al., 2016).

The NR1 subfamily of nuclear hormone receptors (NRs) heterodimerize with retinoid X receptors (RXRs) to either promote (pregnane X receptor (PXR) or liver X receptor (LXR)) or inhibit (peroxisome proliferator-activated receptors (PPARs), constitutive androstane receptor (CAR), farnesoid X receptor (FXR), and thyroid receptors (TRs)) hepatic steatosis upon binding their naturally occurring agonist ligands. Select endocrine-disrupting chemicals (EDCs) known to bind these NRs and affect their activity.

The aryl hydrocarbon receptor (AhR) is a ligand-activated transcription factor and member of the basic helix-loop-helix PER-ARNT-SIM (bHLH-PAS) and nuclear receptor (NR) superfamilies (Matthews and Ahmed, 2013). The bHLH-PAS and NRs regulate many vital physiological processes including metabolism, circadian rhythm, differentiation, development, and reproduction. The aryl hydrocarbon receptor (AhR) represents the third major NR effector of EDC action in the liver, as a receptor involved in the metabolism of many xenobiotic substances (Swedenborg et al., 2009). Interaction of a compound with the AHR depends on coplanar structure. There is an extensive toxicological literature on the structure and function of the AhR. Some, but not all EDCs, also activate the AhR, thereby exerting multiple physiological effects (Ottinger and Dean, 2010, Lee et al., 2017). Previous studies have proven that POPs such as dioxins, benzo[a]pyrene and some PCBs bind and activate AhR leading to enhanced steatosis. Our result, indicate that phthalates and metals may also interfering with AhR receptor in a similar way.

Constitutive androstane receptor (CAR, NR1I3) is also a member of the superfamily of nuclear receptors. CAR influence on a variety of physiological functions, such as gluconeogenesis, metabolism of xenobiotics, fatty acids, and bile acids, hormonal regulation, etc. Xenobiotics bind and activate CAR; however, species-specific differences clearly exist. For example, 1,4-bis[2-(3,5-

dichloropyridyloxy)]benzene (TCPOBOP) activates the mouse but not the human CAR (Foulds et al., 2017). The presented study revealed that the phthalates, which are under consideration, bind and activate CAR. Further study of CAR activation after exposure to certain EDCs is of practical importance because changes in CAR activity can lead to disorders in physiological processes, which finally can result in changes in pathological states.

Integrated pathway analysis using data derived from untargeted metabolomics and proteomics analysis revealed perturbation in biogenic amino acids metabolism (Biogenic Amine Synthesis/ Dopamine metabolism). Biogenic amines are one of two broad classes of classical neurotransmitters and include: acetylcholine, serotonin, histamine, and the catecholamines epinephrine, norepinephrine, and dopamine. EDCs can disrupt the synthesis, transport, and release of many neurotransmitters, including dopamine, serotonin, norepinephrine, and glutamate, which play key roles in modulating behavior, cognition, learning, and memory. Perturbations on the main pathways of dopamine, serotonin, norepinephrine, and glutamate metabolism could lead to identifying potential biomarkers of neurodevelopment (Schug et al., 2015). Several in vivo studies has shown that Pd, as well as Cd, can caused changes in the hypothalamic concentrations of the biogenic amines epinephrine, norepinephrine, dopamine, and serotonin and their metabolites 3,4 dihydroxyphenylacetic acid, 3-methoxytyramine, homovanillic acid, and 5-hydroxyindol acetic acid (5-HIAA) (Romero et al., 2011, Naz, 2005).

Multi-omics pathway analysis using data derived from untargeted metabolomics and proteomics analysis revealed dysregulation in purine and pyrimidine synthesis and metabolism. More specific, the following metabolic pathways have been perturbated due to the co-exposure to phthtalates and heavy metals: purine nucleotides de novo biosynthesis II/ pyrimidine ribonucleotides de novo biosynthesis/ pyrimidine ribonucleotides interconversion/ uridine-5'-phosphate biosynthesis. In recent years, a substantial body of evidence has emerged demonstrating that purine and pyrimidine synthesis and metabolism play major roles in controlling embryonic and fetal development and organogenesis. ATP is involved in the development of synaptic transmission and contributes to the establishment of functional neuronal networks in the developing brain. The purinergic control of neurodevelopment is not limited to prenatal life, but is maintained in postnatal life, when it plays fundamental roles in controlling oligodendrocyte maturation from precursors and their terminal differentiation to fully myelinating cells. Based on the above-mentioned and other literature evidence, it is now increasingly clear that any defect altering the tight regulation of purinergic transmission and of purine and pyrimidine metabolism during pre- and post-natal brain development may translate into functional deficits, which could be at the basis of severe pathologies characterized by mental retardation or other disturbances. This can occur either at the level of the recruitment and/or signaling of specific nucleotide or nucleoside receptors or through genetic alterations in key steps of the purine salvage pathway (Fumagalli et al., 2017) It has been found that the exposure to phthalates results in a series of metabolites of purine catabolism, such as xanthine, allantoin and urea. The observed increased levels of these metabolites, together with the elevation of uridine, suggest an activation of nucleic acid degradation (Xia et al., 2011).

Another evidence of the dysregulation of energy metabolism, is the identification of NAD biosynthesis II (from tryptophan) after multi-omics pathway analysis using the proteomics and metabolomics results. Mitochondrial dysfunction has now been associated with over 40 major diseases and health problems including type 2 diabetes, cancer, Alzheimer's disease and other neurodegenerative diseases. Mitochondria are intracellular powerhouses that produce ATP and carry out diverse functions for cellular energy metabolism. While the maintenance of an optimal NAD/NADH ratio is essential for mitochondrial function, it has recently become apparent that the maintenance of the mitochondrial NAD pool also has critical importance. The biosynthesis, transport, and catabolism of NAD and its key intermediates play an important role in the regulation of NAD-consuming mediators, such as sirtuins, poly-ADP-ribose polymerases, and CD38/157 ectoenzymes, in intra- and extracellular compartments. Mitochondrial NAD biosynthesis is also modulated in response to nutritional and environmental stimuli (Stein and Imai, 2012).

Choline functions in several important structural and cell signalling roles, which are integral in the formation of VLDL, phospholipids (phosphatidylcholine and sphingomyelin) and the neurotransmitter acetylcholine (ACh). In addition, choline functions as a methyl donor and is crucial for DNA regulation and repair, protein function and intermediary metabolism. Following cellular uptake, choline is phosphorylated to phosphocholine, or irreversibly oxidised to betaine, which functions to donate methyl groups to homocysteine, producing the essential amino acid methionine. Choline can be synthesised endogenously by methylation of phosphatidylethanolamine, a process which occurs primarily in the liver, but also occurs in neuronal cells. However, de novo synthesis alone is not sufficient to meet human requirements. Choline is found naturally in a wide range of foods in the free and esterified form and betaine is also available directly

from the diet (Strain et al., 2013). Fowler et al. 2012 showed that exposure to the phthalate DEHP and its metabolites may cause increase of phosphatidylcholine. In addition, Xu et al. showed that the concentrations of ten lipid classes (cholesterol esters, diacylglycerol, triacylglycerides, phosphatidylcholine, phosphatidylethanolamine, phosphatidylserine, lysophosphatidylcholine, cardiolipin, and sphingomyelin) were determined, as well as the individual fatty acid compositions, especially the omega-3 and omega-6 family of EFAs, based on the on the lipid metabolome in a rat HRP-1 trophoblast model. The level of each lipid class was significantly increased upon exposure to the agents, with MEHP and EHA generally showing higher increases than DEHP (Xu et al., 2006). The results of our study strengthen the aforementioned conclusions, since after the exposure to phthalates and metals, the metabolic pathways phosphatidylcholine biosynthesis I/ phosphatidylethanolamine biosynthesis II have been perturbed according to the multi-omics pathway analysis.

Table 13. Multi-omics pathway analysis based on the transcriptomics and the proteomics results.

Pathways	p-value of Experiment Type (transcriptomics)	Pathway Entities of Experiment Type (transcriptomics)	Matched Entities (transcriptomics)	Pathway Entities of Experiment Type (metabolomics)	Matched Entities (metabolomics)
3-phosphoinositide biosynthesis	1	26	0	26	2
3-phosphoinositide degradation	1	21	0	21	2
4-hydroxy-2-nonenal detoxification	1	5	0	5	2
4-hydroxybenzoate biosynthesis	0.001393	1	1	1	0
4-hydroxyphenylpyruvate biosynthesis	0.001393	1	1	1	0
5-aminoimidazole ribonucleotide biosynthesis I	1	3	0	3	1
Amino sugar and nucleotide sugar metabolism	1	47	0	47	7
Base excision repair	1	33	0	33	1
CDP-diacylglycerol biosynthesis I	1	19	0	19	2
CMP-N-acetylneuraminate biosynthesis I (eukaryotes)	1	4	0	4	1
D-mannose degradation	1	1	0	1	1
D-myo-inositol (1,4,5)-trisphosphate biosynthesis	1	25	0	25	2
D-myo-inositol-5-phosphate metabolism	1	19	0	19	1
DNA replication	1	36	0	36	5
Fatty acid biosynthesis	1	6	0	6	2
GDP-L-fucose biosynthesis I (from GDP-D-mannose)	1	2	0	2	1
GDP-mannose biosynthesis	1	6	0	6	2
Glycolysis / Gluconeogenesis	1	66	0	66	3
AGE-RAGE pathway WP2324 78487	1	66	0	66	7
AMP-activated Protein Kinase (AMPK) Signaling	1	68	0	68	3
ATM Signaling Pathway	1	41	0	41	4
Acetylcholine Synthesis	1	7	0	7	1
Adipogenesis	1	131	0	131	10

Pathways	p-value of Experiment Type (transcriptomics)	Pathway Entities of Experiment Type (transcriptomics)	Matched Entities (transcriptomics)	Pathway Entities of Experiment Type (metabolomics)	Matched Entities (metabolomics)
Allograft Rejection	0.11063	100	1	100	5
Alpha 6 Beta 4 signaling pathway	1	33	0	33	5
Alzheimers Disease	1	149	0	149	10
Amyotrophic lateral sclerosis (ALS)	1	38	0	38	4
Androgen receptor signaling pathway	1	89	0	89	8
Angiogenesis	1	24	0	24	1
Apoptosis-related network due to altered Notch3 in ovarian cancer	1	53	0	53	3
Apoptosis Modulation and Signaling	1	95	0	95	7
Apoptosis Modulation by HSP70	1	20	0	20	2
Apoptosis	1	87	0	87	7
Arrhythmogenic Right Ventricular Cardiomyopathy	1	78	0	78	5
Aryl Hydrocarbon Receptor Pathway	0.001891	46	2	46	4
Aryl Hydrocarbon Receptor	1	48	0	48	2
B Cell Receptor Signaling Pathway	1	98	0	98	6
Benzo(a)pyrene metabolism	1	9	0	9	1
Biogenic Amine Synthesis	1	15	0	15	1
Bladder Cancer	1	31	0	31	3
Brain-Derived Neurotrophic Factor (BDNF) signaling pathway	1	144	0	144	14
Calcium Regulation in the Cardiac Cell	1	150	0	150	7
Cardiac Hypertrophic Response	1	54	0	54	4
Cardiac Progenitor Differentiation	0.071273	53	1	53	0
Catalytic cycle of mammalian Flavin-containing MonoOxygenases (FMOs)	1	5	0	5	1
Cell Cycle	1	103	0	103	7
Cholesterol Biosynthesis	1	15	0	15	3
Circadian rythm related genes	1	210	0	210	12
Codeine and Morphine Metabolism	1	9	0	9	4
Complement Activation	1	22	0	22	2
Complement and Coagulation Cascades	1	61	0	61	4
Composition of Lipid Particles	1	10	0	10	1
Constitutive Androstane Receptor Pathway	1.11E-09	32	5	32	6
Copper homeostasis	1	55	0	55	7
Cori Cycle	1	23	0	23	2

Pathways	p-value of Experiment Type (transcriptomics)	Pathway Entities of Experiment Type (transcriptomics)	Matched Entities (transcriptomics)	Pathway Entities of Experiment Type (metabolomics)	Matched Entities (metabolomics)
Corticotropin-releasing hormone signaling pathway	0.120519	92	1	92	7
Cytoplasmic Ribosomal Proteins	0.115588	88	1	88	8
DDX1 as a regulatory component of the Drosha microprocessor	1	7	0	7	2
DNA Damage Response (only ATM dependent)	1	114	0	114	6
DNA Damage Response	1	68	0	68	4
DNA Replication	1	42	0	42	4
Deregulation of Rab and Rab Effector Genes in Bladder Cancer	1	16	0	16	1
Diclofenac Metabolic Pathway	0.006946	5	1	5	0
Differentiation Pathway	0.064767	50	1	50	0
Differentiation of white and brown adipocyte	0.034262	25	1	25	1
Diurnally Regulated Genes with Circadian Orthologs	1	48	0	48	5
Dopamine metabolism	1	13	0	13	4
Drug Induction of Bile Acid Pathway	0.023425	17	1	17	3
Dual hijack model of Vif in HIV infection	1	8	0	8	2
EBV LMP1 signaling	0.030212	24	1	24	1
EGF-EGFR Signaling Pathway	1	162	0	162	13
EPO Receptor Signaling	1	26	0	26	2
Ectoderm Differentiation	1	145	0	145	4
Effects of Nitric Oxide	1	8	0	8	1
Electron Transport Chain	1	104	0	104	15
Endochondral Ossification	0.084151	64	1	64	2
Endoderm Differentiation	0.176479	146	1	146	8
Endothelin Pathways	1	33	0	33	3
ErbB Signaling Pathway	1	55	0	55	5
Estrogen metabolism	1	18	0	18	4
Estrogen signaling pathway	1	23	0	23	3
Eukaryotic Transcription Initiation	1	41	0	41	3
Extracellular vesicle-mediated signaling in recipient cells	0.040975	30	1	30	1
Factors and pathways affecting insulin-like growth factor (IGF1)-Akt signaling	1	33	0	33	2
Farnesoid X Receptor Pathway	0.026146	19	1	19	1

Pathways	p-value of Experiment Type (transcriptomics)	Pathway Entities of Experiment Type (transcriptomics)	Matched Entities (transcriptomics)	Pathway Entities of Experiment Type (metabolomics)	Matched Entities (metabolomics)
Fas Ligand (FasL) pathway and Stress induction of Heat Shock Proteins (HSP) regulation	1	43	0	43	3
Fatty Acid Beta Oxidation	1	34	0	34	2
Fatty Acid Biosynthesis	1	22	0	22	4
Fatty Acid Omega Oxidation	1.97E-04	15	2	15	1
Fluoropyrimidine Activity	0.044981	34	1	34	4
Focal Adhesion	1	191	0	191	13
Folate-Alcohol and Cancer Pathway	1	8	0	8	1
Folate Metabolism	0.003849	67	2	67	1
Follicle Stimulating Hormone (FSH) signaling pathway	1	27	0	27	2
G13 Signaling Pathway	1	38	0	38	4
G1 to S cell cycle control	1	68	0	68	4
G Protein Signaling Pathways	1	92	0	92	13
Ganglio Sphingolipid Metabolism	1	18	0	18	1
Gastric Cancer Network 1	1	29	0	29	1
L-dopa degradation	1	1	0	1	1
L-serine degradation	1	2	0	2	1
MAPK signaling pathway	0.300102	257	1	257	20
N-Glycan biosynthesis	1	49	0	49	6
NAD biosynthesis II (from tryptophan)	1	10	0	10	1
NAD salvage pathway II	1	13	0	13	1
Oxidative phosphorylation	1	133	0	133	17
PRPP biosynthesis I	1	3	0	3	2
Pathways in cancer	0.366601	327	1	327	22
Porphyrin and chlorophyll metabolism	0.058217	43	1	43	7
S-adenosyl-L-methionine biosynthesis	1	3	0	3	1
S-methyl-5-thio-Alpha-D-ribose 1-phosphate degradation	1	4	0	4	3
UDP-N-acetyl-D-galactosamine biosynthesis II	1	9	0	9	2
UDP-N-acetyl-D-glucosamine biosynthesis II	1	5	0	5	2
acyl-CoA hydrolysis	1	3	0	3	1
adenine and adenosine salvage III	1	4	0	4	1
adenosine nucleotides degradation II	1	7	0	7	3
arginine biosynthesis IV	1	6	0	6	2
asparagine biosynthesis I	1	1	0	1	1

Pathways	p-value of Experiment Type (transcriptomics)	Pathway Entities of Experiment Type (transcriptomics)	Matched Entities (transcriptomics)	Pathway Entities of Experiment Type (metabolomics)	Matched Entities (metabolomics)
cholesterol biosynthesis I	1	13	0	13	3
cholesterol biosynthesis II (via 24,25-dihydrolanosterol)	1	13	0	13	3
cholesterol biosynthesis III (via desmosterol)	1	13	0	13	3
choline biosynthesis III	1	9	0	9	2
citrulline degradation	1	1	0	1	1
coenzyme A biosynthesis	1	3	0	3	1
colanic acid building blocks biosynthesis	1	13	0	13	4
creatine-phosphate biosynthesis	1	5	0	5	1
dolichyl-diphosphooligosaccharide biosynthesis	1	8	0	8	2
dopamine degradation	1	7	0	7	1
fatty acid Alpha-oxidation II	1	9	0	9	2
fatty acid Beta-oxidation I	1	16	0	16	2
fatty acid activation	1	8	0	8	2
fatty acid biosynthesis initiation II	1	3	0	3	1
galactose degradation I (Leloir pathway)	1	4	0	4	1
gluconeogenesis I	1	21	0	21	1
glutamate biosynthesis II	1	2	0	2	1
glutamate degradation X	1	2	0	2	1
glutamine degradation I	1	3	0	3	2
glutathione redox reactions I	1	9	0	9	1
glutathione-mediated detoxification I	0.035608	26	1	26	3
glycerol-3-phosphate shuttle	1	2	0	2	1
glycine biosynthesis III	1	2	0	2	1
guanosine nucleotides degradation III	1	2	0	2	2
heme biosynthesis II	1	9	0	9	2
heme biosynthesis from uroporphyrinogen-III I	1	4	0	4	2
histamine degradation	1	3	0	3	1
inosine-5'-phosphate biosynthesis II	1	3	0	3	1
mevalonate pathway I	1	12	0	12	2
molybdenum cofactor biosynthesis	1	3	0	3	1
noradrenaline and adrenaline degradation	1	9	0	9	1
oleate biosynthesis II (animals)	1	8	0	8	1
phenylalanine degradation I (aerobic)	1	6	0	6	1

Pathways	p-value of Experiment Type (transcriptomics)	Pathway Entities of Experiment Type (transcriptomics)	Matched Entities (transcriptomics)	Pathway Entities of Experiment Type (metabolomics)	Matched Entities (metabolomics)
phosphatidylcholine biosynthesis I	1	6	0	6	1
phosphatidylethanolamine biosynthesis II	1	6	0	6	1
phosphatidylglycerol biosynthesis II (non-plastidic)	1	20	0	20	2
phospholipases	1	38	0	38	2
proline biosynthesis I	1	4	0	4	1
proline biosynthesis II (from arginine)	1	5	0	5	1
purine nucleotides de novo biosynthesis II	1	9	0	9	4
purine nucleotides degradation II (aerobic)	1	10	0	10	5
purine ribonucleosides degradation to ribose-1-phosphate	1	2	0	2	1
pyrimidine ribonucleotides de novo biosynthesis	1	14	0	14	3
pyrimidine ribonucleotides interconversion	1	12	0	12	2
pyruvate fermentation to lactate	1	5	0	5	1
salvage pathways of pyrimidine deoxyribonucleotides	1	5	0	5	1
salvage pathways of pyrimidine ribonucleotides	1	15	0	15	1
stearate biosynthesis I (animals)	1	13	0	13	3
sulfate activation for sulfonation	1	2	0	2	1
sulfite oxidation IV	1	1	0	1	1
superpathway of cholesterol biosynthesis	1	27	0	27	5
superpathway of geranylgeranyldiphosphate biosynthesis I (via mevalonate)	1	14	0	14	2
superpathway of inositol phosphate compounds	1	67	0	67	3
tRNA charging	1	38	0	38	7
thio-molybdenum cofactor biosynthesis	1	1	0	1	1
thymine degradation	1	8	0	8	2
triacylglycerol biosynthesis	1	27	0	27	2
tryptophan degradation III (eukaryotic)	1	11	0	11	1
tryptophan degradation to 2-amino-3-carboxymuconate semialdehyde	1	5	0	5	1
tyrosine degradation I	0.00833	6	1	6	0
uracil degradation II (reductive)	1	8	0	8	2
urate biosynthesis/inosine 5'-phosphate degradation	1	5	0	5	2
urea cycle	0.00833	6	1	6	1
uridine-5'-phosphate biosynthesis	1	2	0	2	1

Pathways	p-value of Experiment Type (transcriptomics)	Pathway Entities of Experiment Type (transcriptomics)	Matched Entities (transcriptomics)	Pathway Entities of Experiment Type (metabolomics)	Matched Entities (metabolomics)
zymosterol biosynthesis	1	6	0	6	2

Table 14. Multi-omics pathway analysis based on the proteomics and metabolomics results.

Pathways	Pathway Entities of Experiment Type (proteoomics)	Matched Entities (proteomics)	Pathway Entities of Experiment Type (metabolomics)	Matched Entities (metabolomics)
(S)-reticuline biosynthesis II	0	1	1	16
3-phosphoinositide biosynthesis	2	26	0	15
3-phosphoinositide degradation	2	21	0	9
4-aminobutyrate degradation I	0	2	1	9
4-hydroxy-2-nonenal detoxification	2	5	2	8
4-hydroxybenzoate biosynthesis	0	1	1	18
4-hydroxyphenylpyruvate biosynthesis	0	1	1	4
4-hydroxyproline degradation I	0	1	1	13
5-aminoimidazole ribonucleotide biosynthesis I	1	3	2	17
Amino sugar and nucleotide sugar metabolism	7	47	1	99
Base excision repair	1	33	0	0
Beta-alanine degradation I	0	2	1	9
CDP-diacylglycerol biosynthesis I	2	19	1	12
CMP-N-acetylneuraminate biosynthesis I (eukaryotes)	1	4	0	14
D-mannose degradation	1	1	0	2
D-myo-inositol (1,4,5)-trisphosphate biosynthesis	2	25	0	13
D-myo-inositol-5-phosphate metabolism	1	19	0	10

Pathways	Pathway Entities of Experiment Type (proteoomics)	Matched Entities (proteomics)	Pathway Entities of Experiment Type (metabolomics)	Matched Entities (metabolomics)
DNA replication	5	36	0	0
Fatty acid biosynthesis	2	6	0	49
GDP-L-fucose biosynthesis I (from GDP-D-mannose)	1	2	0	7
GDP-mannose biosynthesis	2	6	0	8
Gamma-glutamyl cycle	0	11	3	15
Glycolysis / Gluconeogenesis	3	66	0	31
AGE-RAGE pathway	7	66	0	0
AMP-activated Protein Kinase (AMPK) Signaling	3	68	0	7
ATM Signaling Pathway	4	41	0	0
Acetylcholine Synthesis	1	7	0	10
Adipogenesis	10	131	0	0
Allograft Rejection	5	100	0	10
Alpha 6 Beta 4 signaling pathway	5	33	0	0
Alzheimers Disease	10	149	0	7
Amino acid conjugation	0	0	1	5
Amyotrophic lateral sclerosis (ALS)	4	38	1	12
Androgen receptor signaling pathway	8	89	0	0
Angiogenesis	1	24	0	0
Apoptosis-related network due to altered Notch3 in ovarian cancer	3	53	0	0
Apoptosis Modulation and Signaling	7	95	0	1
Apoptosis Modulation by HSP70	2	20	0	0
Apoptosis	7	87	0	0

Pathways	Pathway Entities of Experiment Type (proteoomics)	Matched Entities (proteomics)	Pathway Entities of Experiment Type (metabolomics)	Matched Entities (metabolomics)
Arrhythmogenic Right Ventricular Cardiomyopathy	5	78	0	2
Aryl Hydrocarbon Receptor Pathway	4	46	0	1
Aryl Hydrocarbon Receptor	2	48	0	2
B Cell Receptor Signaling Pathway	6	98	0	0
Benzo(a)pyrene metabolism	1	9	0	7
Biogenic Amine Synthesis	1	15	1	17
Bladder Cancer	3	31	0	0
Brain-Derived Neurotrophic Factor (BDNF) signaling pathway	14	144	0	4
Calcium Regulation in the Cardiac Cell	7	150	0	12
Cardiac Hypertrophic Response	4	54	0	6
Catalytic cycle of mammalian Flavin-containing MonoOxygenases (FMOs)	1	5	0	7
Cell Cycle	7	103	0	0
Cholesterol Biosynthesis	3	15	0	15
Circadian rythm related genes	12	210	0	0
Codeine and Morphine Metabolism	4	9	0	7
Complement Activation	2	22	0	1
Complement and Coagulation Cascades	4	61	0	2
Composition of Lipid Particles	1	10	0	10
Constitutive Androstane Receptor Pathway	6	32	0	1
Copper homeostasis	7	55	0	2
Cori Cycle	2	23	0	15
Corticotropin-releasing hormone signaling pathway	7	92	0	0

Pathways	Pathway Entities of Experiment Type (proteoomics)	Matched Entities (proteomics)	Pathway Entities of Experiment Type (metabolomics)	Matched Entities (metabolomics)
Cytoplasmic Ribosomal Proteins	8	88	0	0
DDX1 as a regulatory component of the Drosha microprocessor	2	7	0	0
DNA Damage Response (only ATM dependent)	6	114	0	0
DNA Damage Response	4	68	0	4
DNA Replication	4	42	0	7
Deregulation of Rab and Rab Effector Genes in Bladder Cancer	1	16	0	0
Differentiation of white and brown adipocyte	1	25	0	0
Diurnally Regulated Genes with Circadian Orthologs	5	48	0	0
Dopamine metabolism	4	13	1	34
Drug Induction of Bile Acid Pathway	3	17	0	27
Dual hijack model of Vif in HIV infection	2	8	0	0
EBV LMP1 signaling	1	24	0	0
EGF-EGFR Signaling Pathway	13	162	0	0
EPO Receptor Signaling	2	26	0	0
Ectoderm Differentiation	4	145	0	0
Effects of Nitric Oxide	1	8	0	7
Electron Transport Chain	15	104	0	12
Endochondral Ossification	2	64	0	4
Endoderm Differentiation	8	146	0	0
Endothelin Pathways	3	33	0	13
ErbB Signaling Pathway	5	55	0	2
Estrogen metabolism	4	18	2	18

Pathways	Pathway Entities of Experiment Type (proteoomics)	Matched Entities (proteomics)	Pathway Entities of Experiment Type (metabolomics)	Matched Entities (metabolomics)
Estrogen signaling pathway	3	23	0	2
Eukaryotic Transcription Initiation	3	41	0	0
Extracellular vesicle-mediated signaling in recipient cells	1	30	0	0
Factors and pathways affecting insulin-like growth factor (IGF1)-Akt signaling	2	33	0	0
Farnesoid X Receptor Pathway	1	19	0	1
Fas Ligand (FasL) pathway and Stress induction of Heat Shock Proteins (HSP) regulation	3	43	1	3
Fatty Acid Beta Oxidation	2	34	0	33
Fatty Acid Biosynthesis	4	22	0	8
Fatty Acid Omega Oxidation	1	15	1	3
Fluoropyrimidine Activity	4	34	0	8
Focal Adhesion	13	191	0	0
Folate-Alcohol and Cancer Pathway	1	8	0	13
Folate Metabolism	1	67	0	72
Follicle Stimulating Hormone (FSH) signaling pathway	2	27	0	0
G13 Signaling Pathway	4	38	0	0
G1 to S cell cycle control	4	68	0	0
G Protein Signaling Pathways	13	92	0	4
Ganglio Sphingolipid Metabolism	1	18	0	18
Gastric Cancer Network 1	1	29	0	0
L-cysteine degradation I	0	2	1	10
L-cysteine degradation III	0	1	1	8
L-dopa degradation	1	1	1	12

Pathways	Pathway Entities of Experiment Type (proteoomics)	Matched Entities (proteomics)	Pathway Entities of Experiment Type (metabolomics)	Matched Entities (metabolomics)
L-glutamine biosynthesis II (tRNA-dependent)	0	2	2	10
L-serine degradation	1	2	0	4
MAPK signaling pathway	20	257	0	5
N-Glycan biosynthesis	6	49	0	36
NAD biosynthesis II (from tryptophan)	1	10	2	24
NAD biosynthesis from 2-amino-3-carboxymuconate semialdehyde	0	5	2	14
NAD salvage pathway II	1	13	0	11
Oxidative phosphorylation	17	133	0	16
PRPP biosynthesis I	2	3	0	5
Pathways in cancer	22	327	1	20
Porphyrin and chlorophyll metabolism	7	43	1	124
S-adenosyl-L-methionine biosynthesis	1	3	0	6
S-methyl-5-thio-Alpha-D-ribose 1-phosphate degradation	3	4	0	14
UDP-D-xylose and UDP-D-glucuronate biosynthesis	0	2	1	8
UDP-N-acetyl-D-galactosamine biosynthesis I	0	1	1	2
UDP-N-acetyl-D-galactosamine biosynthesis II	2	9	1	17
UDP-N-acetyl-D-glucosamine biosynthesis II	2	5	2	12
acyl-CoA hydrolysis	1	3	0	3
adenine and adenosine salvage III	1	4	0	11
adenosine nucleotides degradation II	3	7	0	13
alanine biosynthesis II	0	2	1	4
alanine degradation III	0	2	1	4

Pathways	Pathway Entities of Experiment Type (proteoomics)	Matched Entities (proteomics)	Pathway Entities of Experiment Type (metabolomics)	Matched Entities (metabolomics)
arginine biosynthesis IV	2	6	1	22
arginine degradation I (arginase pathway)	0	4	1	11
arginine degradation VI (arginase 2 pathway)	0	6	1	12
asparagine biosynthesis I	1	1	2	9
aspartate biosynthesis	0	3	1	4
aspartate degradation II	0	5	1	8
cholesterol biosynthesis I	3	13	0	33
cholesterol biosynthesis II (via 24,25-dihydrolanosterol)	3	13	0	33
cholesterol biosynthesis III (via desmosterol)	3	13	0	33
choline biosynthesis III	2	9	2	11
citrulline degradation	1	1	0	9
coenzyme A biosynthesis	1	3	0	13
colanic acid building blocks biosynthesis	4	13	1	24
creatine-phosphate biosynthesis	1	5	1	5
dolichyl-diphosphooligosaccharide biosynthesis	2	8	1	23
dopamine degradation	1	7	0	17
fatty acid Alpha-oxidation II	2	9	0	14
fatty acid Beta-oxidation I	2	16	0	15
fatty acid activation	2	8	0	6
fatty acid biosynthesis initiation II	1	3	0	3
folate polyglutamylation	0	5	1	12
formaldehyde oxidation II (glutathione-dependent)	0	2	1	9
galactose degradation I (Leloir pathway)	1	4	1	11

Pathways	Pathway Entities of Experiment Type (proteoomics)	Matched Entities (proteomics)	Pathway Entities of Experiment Type (metabolomics)	Matched Entities (metabolomics)
gluconeogenesis I	1	21	0	23
glutamate biosynthesis II	1	2	1	7
glutamate degradation II	0	3	1	7
glutamate degradation III (via 4-aminobutyrate)	0	4	1	10
glutamate degradation X	1	2	1	7
glutamate dependent acid resistance	0	2	1	4
glutamate removal from folates	0	1	1	3
glutamine biosynthesis I	0	2	2	6
glutamine degradation I	2	3	2	5
glutathione biosynthesis	0	1	2	9
glutathione redox reactions I	1	9	1	9
glutathione-mediated detoxification I	3	26	2	14
glycerol-3-phosphate shuttle	1	2	0	5
glycine biosynthesis III	1	2	0	4
guanosine nucleotides degradation III	2	2	0	12
heme biosynthesis II	2	9	0	18
heme biosynthesis from uroporphyrinogen-III I	2	4	0	11
histamine degradation	1	3	1	18
histidine degradation III	0	7	1	12
inosine-5'-phosphate biosynthesis II	1	3	0	16
leukotriene biosynthesis	0	4	1	13
lysine degradation II	0	3	1	17
methylglyoxal degradation I	0	3	1	7

Pathways	Pathway Entities of Experiment Type (proteoomics)	Matched Entities (proteomics)	Pathway Entities of Experiment Type (metabolomics)	Matched Entities (metabolomics)
mevalonate pathway I	2	12	0	17
molybdenum cofactor biosynthesis	1	3	0	13
noradrenaline and adrenaline degradation	1	9	0	20
oleate biosynthesis II (animals)	1	8	0	7
phenylalanine degradation I (aerobic)	1	6	0	10
phosphatidylcholine biosynthesis I	1	6	1	11
phosphatidylethanolamine biosynthesis II	1	6	0	11
phosphatidylglycerol biosynthesis II (non-plastidic)	2	20	1	17
phospholipases	2	38	2	12
proline biosynthesis I	1	4	1	14
proline biosynthesis II (from arginine)	1	5	1	16
purine nucleotides de novo biosynthesis II	4	9	2	33
purine nucleotides degradation II (aerobic)	5	10	0	19
purine ribonucleosides degradation to ribose-1-phosphate	1	2	0	13
pyrimidine ribonucleotides de novo biosynthesis	3	14	2	25
pyrimidine ribonucleotides interconversion	2	12	2	13
pyruvate fermentation to lactate	1	5	0	5
salvage pathways of pyrimidine deoxyribonucleotides	1	5	0	14
salvage pathways of pyrimidine ribonucleotides	1	15	0	19
serine biosynthesis	0	3	1	11
sphingomyelin metabolism	0	8	1	9
stearate biosynthesis I (animals)	3	13	0	17
sulfate activation for sulfonation	1	2	0	7

Pathways	Pathway Entities of Experiment Type (proteoomics)	Matched Entities (proteomics)	Pathway Entities of Experiment Type (metabolomics)	Matched Entities (metabolomics)
sulfite oxidation IV	1	1	0	5
superpathway of cholesterol biosynthesis	5	27	0	63
superpathway of geranylgeranyldiphosphate biosynthesis I (via mevalonate)	2	14	0	21
superpathway of inositol phosphate compounds	3	67	0	32
superpathway of serine and glycine biosynthesis I	0	5	1	14
tRNA charging	7	38	2	25
thio-molybdenum cofactor biosynthesis	1	1	0	6
thymine degradation	2	8	0	10
triacylglycerol biosynthesis	2	27	2	13
tryptophan degradation III (eukaryotic)	1	11	0	28
tryptophan degradation to 2-amino-3-carboxymuconate semialdehyde	1	5	0	13
tyrosine degradation I	0	6	1	13
uracil degradation II (reductive)	2	8	0	10
urate biosynthesis/inosine 5'-phosphate degradation	2	5	0	11
urea cycle	1	6	0	17
uridine-5'-phosphate biosynthesis	1	2	2	20
zymosterol biosynthesis	2	6	0	22

3.4 OMICS results of in vitro experiments in in HT-22 cells

More than 3000 proteins were identified and relatively quantified from the four replicate analyses. Different proteins presented significant changes in abundance depending on the metal treatment. For the MeHg exposure, 709 proteins presented changes in the abundance higher than two fold (FC ≥2.0; Ratio≥2 or ≤0.5; p value ≤ 0.05). 289 were upregulated and 420 were downregulated. For As exposure, we

found 672 proteins with significant changes in abundance (FC FC ≥2.0; Ratio≥2 or ≤0.5; p value ≤ 0.05). 363 were upregulated and 309 were downregulated. Finally, for Pb exposure, 80 proteins were found to be significantly upregulated and 74 were downregulated. In total, 154 protein presented significant changes in abundance due to Pb exposure (FC ≥2.0; Ratio≥2 or ≤0.5; p value ≤ 0.05). All these proteins are listed in the Annex Excel file (Excel database).

The figure 4 shows a Venn diagram with the proteins differentially expressed due to the exposure to the three metals. More than 450 proteins changed under both MeHg and As treatments. Table 15 summarize the results of pathway analysis that was performed in order to find out towhich pathways the deregulated proteins belong to. The 10 most enriched ones are presented. Figure 4 shows the biological processes in which the deregulated proteins are grouped in, according to Gene ontology enrichment analysis (GO) Data was analyzed with String tools and proteins re grouped according to the KEGG Pathways they are enriched in. The 154 proteins present in the Pb exposure were not enriched in any KEGG pathway.

In the table 16 are described the Kegg pathways formed by the proteins that were exclusively present in As and MeHg exposures (105 and 221 proteins, respectively).

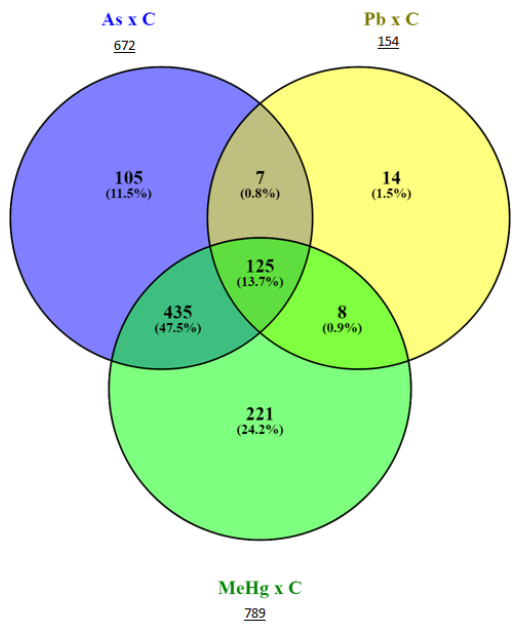

Figure 2: Venn diagram with the proteins differentially expressed due to As, Pb and MeHg treatment.

Table 15. Description of the KEGG[1] Pathways to which deregulated proteins related to the exposure for MeHg and As belong to.

# KEGG Pathway ID	Pathway description	Observed gene count MeHg	False discovery rate MeHg	Observed gene count As	false discovery rate As
1100	Metabolic pathways	90	1,63E-12	77	1,10E-08
3040	Spliceosome	29	3,62E-15	27	7,48E-14
1120	Microbial metabolism in diverse environments	27	2,41E-10	22	2,68E-07
3013	RNA transport	25	1,93E-09	26	1,59E-10
1200	Carbon metabolism	20	5,48E-09	17	6,11E-07
4141	Protein processing in endoplasmic reticulum	20	5,91E-06	18	3,66E-05
5205	Proteoglycans in cancer	19	5,65E-04	21	3,96E-05
4510	Focal adhesion	18	7,28E-04	17	1,47E-03
5016	Huntington s disease	17	3,90E-04	12	3,00E-02
3015	mRNA surveillance pathway	17	8,20E-08	12	1,75E-04
4810	Regulation of actin cytoskeleton	17	2,93E-03	14	2,40E-02

# KEGG Pathway ID	Pathway description	Observed gene count MeHg	False discovery rate MeHg	Observed gene count As	false discovery rate As
5012	Parkinson s disease	16	1,17E-04	12	7,19E-03
5010	Alzheimer s disease	15	1,53E-03	12	1,94E-02
4611	Platelet activation	15	1,69E-04	12	4,21E-03
3010	Ribosome	15	1,17E-04	17	3,89E-06
10	Glycolysis / Gluconeogenesis	14	1,96E-07	11	3,66E-05
280	Valine, leucine and isoleucine degradation	12	1,04E-06	10	3,66E-05
5100	Bacterial invasion of epithelial cells	11	2,54E-04	9	3,70E-03
1230	Biosynthesis of amino acids	11	2,34E-04	11	1,67E-04
71	Fatty acid degradation	11	2,85E-06	12	2,68E-07
1212	Fatty acid metabolism	11	7,46E-06	12	6,11E-07
3008	Ribosome biogenesis in eukaryotes	11	3,12E-04	14	1,53E-06

# KEGG Pathway ID	Pathway description	Observed gene count MeHg	False discovery rate MeHg	Observed gene count As	false discovery rate As
3018	RNA degradation	-		11	1,67E-04
4910	Insulin signaling pathway	10	4,19E-02	11	1,50E-02
620	Pyruvate metabolism	10	1,08E-05	8	3,49E-04
330	Arginine and proline metabolism	10	1,39E-04	-	
3050	Proteasome	9	1,03E-04	10	9,48E-06
640	Propanoate metabolism	8	6,92E-05	5	1,42E-02
410	beta-Alanine metabolism	7	3,98E-04	5	1,42E-02
30	Pentose phosphate pathway	7	3,58E-04	7	3,11E-04
900	Terpenoid backbone biosynthesis	7	4,61E-05	6	3,35E-04
20	Citrate cycle (TCA cycle)	7	4,0E-04	-	

Table 16. KEGG Pathways enriched in deregulated proteins found exclusively in the exposure for As or MeHg.

# KEGG Pathway ID	Pathway description	Observed gene count	False discovery rate
As			
3013	RNA transport	8	1,98E-04
4722	Neurotrophin signaling pathway	5	2,79E-02
MeHg			
1100	Metabolic pathways	31	2,38E-04
3015	mRNA surveillance pathway	7	3,67E-03
1120	Microbial metabolism in diverse environments	9	3,79E-03
4120	Ubiquitin mediated proteolysis	8	3,79E-03
1200	Carbon metabolism	7	4,80E-03
3013	RNA transport	8	8,28E-03
20	Citrate cycle (TCA cycle)	4	8,97E-03
3030	DNA replication	4	1,27E-02
4962	Vasopressin-regulated water reabsorption	4	2,73E-02
4141	Protein processing in endoplasmic reticulum	7	3,33E-02

230	Purine metabolism	7	3,85E-02
5016	Huntington s disease	7	3,90E-02

Comparison between metabolomic biomarkers in human samples and in vitro data

Carnitine is a metabolite found in the study of the cohorts, as well as the L-carnitine biosynthesis pathway in relation with several other metabolites (see excel table, metabolomics sheet) linked with exposure to 13 phthalates and heavy metals. In the in vitro study in HepaRG cells, the expression of a gene involved in carnitine synthesis, BBOX1 (gamma butyrobetaine hydroxylase) is more than 1.5-fold increased after treatment of HepaRG cells with both M1 and M2 mixtures. Indeed, carnitine is important for energy metabolism in link with fatty acid transport in the mitochondria (Rigault et al, 2013). Carnitine deficiency can lead to mitochondrial disease in link with neurodevelopmental disorders (Frye, 2015) and this should be put into perspective with the epidemiological studies which show association between exposure to phthalates and/or metals with neurological diseases (Polanska et al, 2014). Moreover, a homozygous deletion of the BBOX1 and fibin genes has been linked to microcephaly, speech delay, growth retardation and minor facial anomalies (Rashidi-Nezhad et al, 2014).

Fetuin A, encoded by the AHSG gene, is a pleotrophic hepatokine with both pro- and anti-inflammatory actions depending on the tissue. Its mRNA expression is more than 3-fold decreased after treatment of HepaRG cells with either M1 or M2 mixtures. Whereas AHSG increased expression is a risk factor for diabetes and fatty liver disease, its expression promotes wound healing and is neuroprotective in Alzheimer's disease. Decreased fetuin A is associated with an increased disease activity during obstructive lung disease, Crohn's disease and ulcerative colitis (Mukhopadhyay et al, 2014). Indeed, lipid homeostasis and glucose metabolism are pathways dysregulated in link with several metabolites modified in the study of the REPRO_PL and PHIME cohorts, in relation with the levels of phthalates and heavy metals in the human biological samples (see excel table, metabolomics sheet).

4 Discussion and conclusion and current perspectives

The aim of this deliverable is to produce a database of candidate, in vitro supported, -omics derived biomarkers, for targeted analysis. The pollutants chosen (phthalates and heavy metals) were selected on the basis of the concentration of those pollutants found in the biological fluids of the REPRO_PL and PHIME cohorts. Previous work has associated exposure to several phthalates with shorter pregnancy duration and decreased head circumference in neonates (Polanska et al., 2016). Prenatal exposure to various chemicals, including mercury, methylmercury and lead has also been linked to various neurological disorders (reviewed in Kelsey et al. 2015; Llop etal., 2017). In order to produce this database, in vitro experiments were carried out on two cell culture lines: Hepa RG and HT 22. These cell lines were treated with a mixture of metals and phthalates (HepaRG), and metals (HT 22), because the two selected cohorts (REPRO_PL and PHIME) also studied these chemical stressors in relation with cognition and because the liver is the main detoxifying organ in the body.

After treating the HepaRG cell line with two concentrations of the mixture, various omics analysis were performed (proteomics, transcriptomics and metabolomics). Unfortunately, the results of the proteomics were just processed in October, 2017 and metabolomics will be processed after the last shipment of the samples (end of October or beginning of November 2017). The transcriptomics analysis showed a number of genes that were either up- or down regulated. Some of these genes have been linked before to various health outcomes, including neurodevelopmental disorders. For some of these genes, regulation by various pathways and/or pollutants have been described.

Dermatopontin (DPT) is down-regulated (more than 2.3-fold decrease by M1 and M2 mixtures) in the HepaRG cells. Down-regulation by the PPARα pathway is described and, surprisingly, DPT up-regulation is linked to fibrosis in rodents (Lefebvre et al, 2017). Interestingly, another gene, decorin (DCN) is also down-regulated by the M1 mixture and interactions between DPT and DCN have been described (Kuroda et al., 1999).

BBOX1 was up-regulated after exposure to the mixtures of phthalates and metals in the HepaRG model, whereas exposure to diesel exhaust particles in the human THP1 cellular model decreased expression of this gene (Verheyen et al, 2004). Genes involved in carnitine biosynthesis, including BBOX1, and carnitine uptake are up-regulated by PPARa in the liver (Schlegel et al. 2012). However, the role of this up-regulation in the liver whereas its deficiency can lead to mitochondrial disease in link with neurodevelopmental disorders will need to be addressed. Folate deficiency can lead to decreased carnitine synthesis (Da Silva et al., 2014) and mitochondrial disease in link with neurodevelopmental disorders (Frye, 2015) and this should be put into perspective with the epidemiological studies which show association between exposure to phthalates and/or metals with neurological diseases (Polanska et al, 2014). Indeed, pathway analysis after the metabolomic signature found the cohorts in this study showed that the metabolic pathway of L-carnitine biosynthesis was statistical significant perturbed, may be in link with the occurrence of 2-oxoglutarate and succinate in Repro_PL plasma samples and the presence of L-carnitine in both Repro_PL and PHIME children samples. The folate metabolism was also found modified in the HepaRG cells, through the CRP gene (see Table 9).

The paternally imprinted gene H19 and the maternally imprinted gene SNRPN have their methylation status or their expression modified by various pollutants (often in opposite directions), including methoxychlor, vinclozolin and dioxin (Stouder & Paoloni-Giacobino, 2011; Somm et al, 2013 and for review, Vaiserman, 2014).Lead exposure in early childhood also modifies methylation of H19 but not SNRPN in an epidemiological study (Li et al, 2016). First trimester exposure to phthalate and phenol also alters H19 methylation in the placenta (LaRocca et al, 2014). In the HepaRG cells, we found a 1.5-fold increased expression of SNRPN and a 2-fold decreased one for H19. With bisphenol A, no modification was observed for H19 whereas a loss of imprinting for the maternal SNRPN gene was found in the placenta of mice (Susiarjo et al, 2013).

The inflammation marker CRP (c-reactive protein) was 2.4-fold down-regulated at the mRNA leveli in HepaRG cells by both M1 and M2 mixtures. Surprisingly, exposure to several phthalate monoesters was associated with an up-regulation of the seric CRP whereas oxidized metabolites were inversely correlated with this marker (Ferguson et al, 2011).

In human hepatocytes, DEHP, via the constitutive androstane receptor, increased the expression of CYP2B6 (Eveillard et al, 2009). In the HepaRG cells, both M1 and M2 mixture led to a 1.5-fold increase of its mRNA level.

The HT 22 cell culture was treated with metals and subsequent proteomics analysis was performed.

The transcriptomics and proteomics data have been included in the Excel database of in vitro supported, omics derived, biomarkers, as well as the metabolomics from the human samples.

The idea here is that the biomarkers derived from metabolomics analysis of human samples from the two cohorts selected (REPRO_PL and PHIME) will be corroborated from in vitro toxicogenomics (combination of whole genome transcriptomics, proteomics and metabolomics) performed on relevant cellular models.

Data that still needs to be provided (e.g. metabolomics data for the Hepa RG cell line) will be added to this deliverable as an amendment. This amendment will also discuss how the in vitro supported OMICs data correlates to the biomarkers in human samples.

5 References

Alhowikan AM, Ayadhi LA, Halepoto DM. Secretagogin (SCGN) Plasma Levels and their Association with Cognitive and Social Behavior in Children with Autism Spectrum Disorder (ASD). J Coll Physicians Surg Pak. 2017 Apr;27(4):222-226. doi: 2594.

Amiot A, Dona AC, Wijeyesekera A, Tournigand C, Baumgaertner I, Lebaleur Y, Sobhani I, Holmes E. (1)H NMR Spectroscopy of Fecal Extracts Enables Detection of Advanced Colorectal Neoplasia. J Proteome Res. 2015 4;14(9):3871-81.

Anthérieu S, Chesné C, Li R, Camus S, Lahoz A, Picazo L, Turpeinen M, Tolonen A, Uusitalo J, Guguen-Guillouzo C, Guillouzo A. Stable expression, activity, and inducibility of cytochromes P450 in differentiated HepaRG cells. Drug Metab Dispos. 2010 Mar;38(3):516-25. doi: 10.1124/dmd.109.030197. Epub 2009 Dec 17.

Aroner SA, St-Jules DE, Mukamal KJ, Katz R, Shlipak MG, Criqui MH, Kestenbaum B, Siscovick DS, de Boer IH, Jenny NS, Budoff MJ, Ix JH, Jensen MK1. Fetuin-A, glycemic status, and risk of cardiovascular disease: The Multi-Ethnic Study of Atherosclerosis. Atherosclerosis. 2016 May;248:224-9. doi: 10.1016/j.atherosclerosis.2016.03.029. Epub 2016 Mar 22.

Beaudry, P., Campbell, M., Dang, N. H., Wen, J., Blote, K. & Weljie, A. M. 2016. A Pilot Study on the Utility of Serum Metabolomics in Neuroblastoma Patients and Xenograft Models. Pediatr Blood Cancer, 63, 214-20.

Cobas JC, Bernstein MA, Martín-Pastor M, Tahoces PG. (2006) A new general-purpose fully automatic baseline-correction procedure for 1D and 2D NMR data. J Magn Reson. 183(1):145-51.

Da Silva RP, Kelly KB, Al Rajabi A, Jacobs RL. Novel insights on interactions between folate and lipid metabolism. Biofactors. 2014;40(3):277-83.

Eveillard A, Mselli-Lakhal L, Mogha A, Lasserre F, Polizzi A, Pascussi JM, Guillou H, Martin PG, Pineau T. Di-(2-ethylhexyl)-phthalate (DEHP) activates the constitutive androstane receptor (CAR): a novel signalling pathway sensitive to phthalates. Biochem Pharmacol. 2009 Jun 1;77(11):1735-46. doi: 10.1016/j.bcp.2009.02.023. Epub 2009 Mar 11.

Ferguson KK, Loch-Caruso R, Meeker JD. Urinary phthalate metabolites in relation to biomarkers of inflammation and oxidative stress: NHANES 1999-2006. Environ Res. 2011 Jul;111(5):718-26. doi: 10.1016/j.envres.2011.02.002. Epub 2011 Feb 23.

Fowler PA, Bellingham M, Sinclair KD, Evans NP, Pocar P, Fischer B, et al. Impact of endocrine-disrupting compounds (EDCs) on female reproductive health. Mol Cell Endocrinol. 2012;355(2):231–239.

Frye, R.E. (2015) Metabolic and mitochondrial disorders associated with epilepsy in children with autism spectrum disorder, Epilepsy & behavior : E&B, 47, 147-157.

Fumagalli, M., Lecca, D., Abbracchio, M. P. & Ceruti, S. 2017. Pathophysiological Role of Purines and Pyrimidines in Neurodevelopment: Unveiling New Pharmacological Approaches to Congenital Brain Diseases. Frontiers in Pharmacology, 8, 941.

Jewison T, Su Y, Disfany FM, Liang Y, Knox C, Maciejewski A, Poelzer J, Huynh J, Zhou Y, Arndt D, Djoumbou Y, Liu Y, Deng L, Guo AC, Han B, Pon A, Wilson M, Rafatnia S, Liu P, Wishart DS. SMPDB 2.0: big improvements to the Small Molecule Pathway Database. 2014 Nucleic Acids Res. 42(Database issue):D478-84.

Johansson C, Castoldi AF, Onishchenko N, Manzo L, Vahterd M and Ceccatelli S. Neurobehavioural and Molecular Changes Induced by Methylmercury Exposure During Development. Neurotoxicity Research, 2007, VOL. 11(3,4). pp. 1-20

Jossé R1, Aninat C, Glaise D, Dumont J, Fessard V, Morel F, Poul JM, Guguen-Guillouzo C, Guillouzo A. Long-term functional stability of human HepaRG hepatocytes and use for chronic toxicity and genotoxicity studies. Drug Metab Dispos. 2008 Jun;36(6):1111-8. doi: 10.1124/dmd.107.019901. Epub 2008 Mar 17.

Khandelwal R, Sharma AK, Chadalawada S, Sharma Y. Secretagogin Is a Redox-Responsive Ca2+ Sensor. Biochemistry. 2017 Jan 17;56(2):411-420. doi: 10.1021/acs.biochem.6b00761. Epub 2017 Jan 5.

Kitamura Y, Usami R, Ichihara S, Kida H, Satoh M, Tomimoto H, Murata M, Oikawa S. Plasma protein profiling for potential biomarkers in the early diagnosis of Alzheimer's disease. Neurol Res. 2017 Mar;39(3):231-238. doi: 10.1080/01616412.2017.1281195. Epub 2017 Jan 20.

Kuroda K1, Okamoto O, Shinkai H. Dermatopontin expression is decreased in hypertrophic scar and systemic sclerosis skin fibroblasts and is regulated by transforming growth factor-beta1, interleukin-4, and matrix collagen. J Invest Dermatol. 1999 May;112(5):706-10.

LaRocca J, Binder AM, McElrath TF, Michels KB. The impact of first trimester phthalate and phenol exposure on IGF2/H19 genomic imprinting and birth outcomes. Environ Res. 2014 Aug;133:396-406. doi: 10.1016/j.envres.2014.04.032. Epub 2014 Jun 25.

Lefebvre P, Lalloyer F, Baugé E, Pawlak M, Gheeraert C, Dehondt H, Vanhoutte J, Woitrain E, Hennuyer N, Mazuy C, Bobowski-Gérard M, Zummo FP, Derudas B, Driessen A, Hubens G, Vonghia L, Kwanten WJ, Michielsen P, Vanwolleghem T, Eeckhoute J, Verrijken A, Van Gaal L, Francque S, Staels B. Interspecies NASH disease activity whole-genome profiling identifies a fibrogenic role of PPARα-regulated dermatopontin. JCI Insight. 2017 Jul 6;2(13). pii: 92264

Li Y, Xie C, Murphy SK, Skaar D, Nye M, Vidal AC, Cecil KM, Dietrich KN, Puga A, Jirtle RL, Hoyo C. Lead Exposure during Early Human Development and DNA Methylation of Imprinted Gene Regulatory Elements in Adulthood. Environ Health Perspect. 2016 May;124(5):666-73.

Llop S, Engström K, Ballester F, Franforte E, Alhamdow A, Pisa F, Tratnik JS, Mazej D, Murcia M, Rebagliato M, Bustamante M, Sunyer J, Sofianou-Katsoulis A, Prasouli A, Antonopoulou E, Antoniadou I, Nakou S, Barbone F, Horvat M, Broberg K. Polymorphisms in ABC transporter genes and concentrations of mercury in newborns--evidence from two Mediterranean birth cohorts. PLoS One. 2014 May 15;9(5):e97172. doi: 10.1371/journal.pone.0097172. eCollection 2014.

Foulds, C. E., Treviño, L. S., York, B. & Walker, C. L. 2017. Endocrine-disrupting chemicals and fatty liver disease. Nature reviews. Endocrinology, 13, 445-457.

Lee, H. U., Mcpherson, Z. E., Tan, B., Korecka, A. & Pettersson, S. 2017. Host-microbiome interactions: the aryl hydrocarbon receptor and the central nervous system. Journal of Molecular Medicine, 95, 29-39.

Llop S, Tran V, Ballester F, Barbone F, Sofianou-Katsoulis A, Sunyer J, Engström K, Alhamdow A, Love TM, Watson GE, Bustamante M, Murcia M, Iñiguez C, Shamlaye CF, Rosolen V, Mariuz M, Horvat M, Tratnik JS, Mazej D, van Wijngaarden E, Davidson PW, Myers GJ, Rand MD, Broberg K. CYP3A genes and the association between prenatal methylmercury exposure and neurodevelopment. Environ Int. 2017 Aug;105:34-42. doi: 10.1016/j.envint.2017.04.013. Epub 2017 May 10.

Matthews, J. & Ahmed, S. 2013. Chapter One - AHR- and ER-Mediated Toxicology and Chemoprevention. In: FISHBEIN, J. C. & HEILMAN, J. M. (eds.) Advances in Molecular Toxicology. Elsevier.

Meguid, N.A., et al. (2017) Expression of Reactive Oxygen Species–Related Transcripts in Egyptian Children With Autism, Biomarker Insights, 12, 1177271917691035.

Mukhopadhyay S, Mondal SA, Kumar M, Dutta D. Proinflammatory and antiinflammatory attributes of fetuin-a: a novel hepatokine modulating cardiovascular and glycemic outcomes in metabolic syndrome. Endocr Pract. 2014 Dec;20(12):1345-51

Naz, R. K. 2005. Endocrine disruptors: Effects on Male and Female Reproductive Systems. CRC PRESS.

Niska K, Santos-Martinez MJ, Radomski MW, Inkielewicz-Stepniak I. CuO nanoparticles induce apoptosis by impairing the antioxidant defense and detoxification systems in the mouse hippocampal HT22 cell line: protective effect of crocetin. Toxicol In Vitro. 2015 ;29(4):663-71.

Ottinger, M. A. & Dean, K. 2010. Vertebrate Endocrine Disruption A2 - Breed, Michael D. In: MOORE, J. (ed.) Encyclopedia of Animal Behavior. Oxford: Academic Press.

Pohodich, A.E. and Zoghbi, H.Y. (2015) Rett syndrome: disruption of epigenetic control of postnatal neurological functions, Human molecular genetics, 24, R10-16.

Polanska K, Ligocka D, Sobala W, Hanke W. Phthalate exposure and child development: the Polish Mother and Child Cohort Study. Early Hum Dev. 2014 Sep;90(9):477-85

Raju CS, Spatazza J, Stanco A, Larimer P, Sorrells SF, Kelley KW, Nicholas CR, Paredes MF, Lui JH, Hasenstaub AR6, Kriegstein AR, Alvarez-Buylla A, Rubenstein JL, Oldham MC. Secretagogin is Expressed by Developing Neocortical GABAergic Neurons in Humans but not Mice and Increases Neurite Arbor Size and Complexity. Cereb Cortex. 2017 Apr 26:1-13. doi: 10.1093/cercor/bhx101. [Epub ahead of print]

Rashidi-Nezhad A, Talebi S, Saebnouri H, Akrami SM1, Reymond A. The effect of homozygous deletion of the BBOX1 and Fibin genes on carnitine level and acyl carnitine profile. BMC Med Genet. 2014 Jul 1;15:75. doi: 10.1186/1471-2350-15-75.

Reza Sailani M, Jahanbani F, Nasiri J, Behnam M, Salehi M, Sedghi M, Hoseinzadeh M, Takahashi S, Zia A, Gruber J, Lynch JL, Lam D, Winkelmann J, Amirkiai S, Pang B, Rego S, Mazroui S, Bernstein JA, Snyder MP. Association of AHSG with alopecia and mental retardation (APMR) syndrome. Hum Genet. 2017 Mar;136(3):287-296. doi: 10.1007/s00439-016-1756-5. Epub 2017 Jan 4.

Rigault C, Le Borgne F, Tazir B, Benani A, Demarquoy J. A high-fat diet increases L-carnitine synthesis through a differential maturation of the Bbox1 mRNAs. Biochim Biophys Acta. 2013 Feb;1831(2):370-7. doi: 10.1016/j.bbalip.2012.10.007. Epub 2012 Nov 2.

Romero, A., Caride, A., Pereiro, N. & Lafuente, A. 2011. Modulatory Effects of Melatonin on Cadmium-Induced Changes in Biogenic Amines in Rat Hypothalamus.

Schlegel G, Keller J, Hirche F, Geissler S, Schwarz FJ, Ringseis R, Stangl GI, Eder K. Expression of genes involved in hepatic carnitine synthesis and uptake in dairy cows in the transition period and at different stages of lactation. BMC Vet Res. 2012 Mar 14;8:28.

Schug TT, Blawas AM, Gray K, Heindel JJ, Lawler CP. Elucidating the links between endocrine disruptors and neurodevelopment. Endocrinology. 2015. 156(6):1941-51.

Smith CA, I'Maille G, Want EJ, Qin C, Trauger SA, Brandon TR, Custodio DE, Abagyan R, Siuzdak G . METLIN: a metabolite mass spectral database. Ther Drug Monit. 2005 27 : 747–51.{Beaudry, 2016 #280}

Somm E, Stouder C, Paoloni-Giacobino A. Effect of developmental dioxin exposure on methylation and expression of specific imprinted genes in mice. Reprod Toxicol. 2013 Jan;35:150-5. doi: 10.1016/j.reprotox.2012.10.011. Epub 2012 Nov 8.

Stein, L. R. & Imai, S.-I. 2012. The dynamic regulation of NAD metabolism in mitochondria. Trends in endocrinology and metabolism: TEM, 23, 420-428.

Stouder C, Paoloni-Giacobino A. Specific transgenerational imprinting effects of the endocrine disruptor methoxychlor on male gametes. Reproduction. 2011 Feb;141(2):207-16

Strain, J. J., Mcsorley, E. M., Van Wijngaarden, E., Kobrosly, R. W., Bonham, M. P., Mulhern, M. S., Mcafee, A. J., Davidson, P. W., Shamlaye, C. F., Henderson, J., Watson, G. E., Thurston, S. W., Wallace, J. M. W., Ueland, P. M. & Myers, G. J. 2013. Choline status and neurodevelopmental outcomes at 5 years of age in the Seychelles Child Development Nutrition Study. The British journal of nutrition, 110, 330-336.

Susiarjo M, Sasson I, Mesaros C, Bartolomei MS. Bisphenol a exposure disrupts genomic imprinting in the mouse PLoS Genet. 2013 Apr;9(4):e1003401. doi: 10.1371/journal.pgen.1003401. Epub 2013 Apr 4.

Swedenborg, E., Ruegg, J., Makela, S. & Pongratz, I. 2009. Endocrine disruptive chemicals: mechanisms of action and involvement in metabolic disorders. J Mol Endocrinol, 43, 1-10.

Vaiserman A. Early-life Exposure to Endocrine Disrupting Chemicals and Later-life Health Outcomes: An Epigenetic Bridge? Aging Dis. 2014 Jan 28;5(6):419-29. doi: 10.14336/AD.2014.0500419. eCollection 2014 Dec.

Verheyen GR, Nuijten JM, Van Hummelen P, Schoeters GR. Microarray analysis of the effect of diesel exhaust particles on in vitro cultured macrophages. Toxicol In Vitro. 2004 Jun;18(3):377-91.

Wishart DS, Jewison T, Guo AC, Wilson M, Knox C, Liu Y, Djoumbou Y, Mandal R, Aziat F, Dong E, Bouatra S, Sinelnikov I, Arndt D, Xia J, Liu P, Yallou F, Bjorndahl T, Perez-Pineiro R, Eisner R, Allen F, Neveu V, Greiner R, Scalbert A. HMDB 3.0--The Human Metabolome Database in 2013. 2013 Nucleic Acids Res. (Database issue):D801-7.

Wisniewski JR, Zougman A, Nagaraj N, Mann M. Universal sample preparation method for proteome analysis. Nature Methods 2009, VOL.6 NO.5 : 359-62. DOI:10.1038/nmeth.1322.

Worth RG, Esper RM, Warra NS, Kindzelskii AL, Rosenspire AL, Todd RF 3rd, Petty HR. Mercury inhibition of neutrophil activity: evidence of aberrant cellular signalling and incoherent cellular metabolism. Scand J Immunol. 2001 Jan;53(1):49-55.

Xia, H., Chi, Y., Qi, X., Su, M., Cao, Y., Song, P., Li, X., Chen, T.-L., Zhao, A., Zhang, Y., Cao, Y., Ma, X. & Jia, W. 2011. Metabolomic evaluation of di-n-butyl phthalate-induced teratogenesis in mice.

Xu, Y., Knipp, G. T. & Cook, T. J. 2006. Effects of di-(2-ethylhexyl)-phthalate and its metabolites on the lipid profiling in rat HRP-1 trophoblast cells. Arch Toxicol, 80, 293-8.

Yang SY, Lee JJ, Lee JH, Lee K, Oh SH, Lim YM, Lee MS, Lee KJ. Secretagogin affects insulin secretion in pancreatic β-cells by regulating actin dynamics and focal adhesion. Biochem J. 2016 Jun 15;473(12):1791-803. doi: 10.1042/BCJ20160137. Epub 2016 Apr 19.

Yoshimi, N., et al. (2016) Blood metabolomics analysis identifies abnormalities in the citric acid cycle, urea cycle, and amino acid metabolism in bipolar disorder, BBA clinical, 5, 151-158.

Zhen Y, Krausz KW, Chen C, Idle JR, Gonzalez FJ. Metabolomic and genetic analysis of biomarkers for peroxisome proliferator-activated receptor alpha expression and activation. Mol Endocrinol. 2007 21(9):2136-51.

Zheng, X., et al. (2011) Metabolic signature of pregnant women with neural tube defects in offspring, Journal of proteome research, 10, 4845-4854.